STUDIES ON PREPARATIONS AND PHOTOELECTROCHEMICAL PROPERTIES OF SURFACE-MODIFIED SEMICONDUCTOR MICROCRYSTALS

（表面修飾した半導体超微粒子の調製と光電気化学特性に関する研究）

1994

TSUKASA TORIMOTO

Department of Applied Chemistry
Faculty of Engineering
Osaka University

Preface

The work of this thesis was carried out under the guidance of Professor Dr. Hiroshi Yoneyama at Department of Applied Chemistry, Faculty of Engineering, Osaka University.

The objective of this thesis is to characterize surface structures of size-quantized semiconductor microcrystals modified with thiol compounds, and to investigate the influence of the surface structures on the photoinduced charge transfer. Furthermore, attempts are made to attach novel functions to semiconductor microcrystals with surface modification methods. The author hopes that the findings obtained in this work will benefit in progress in photochemistry of semiconductor microcrystals.

Tsukasa Torimoto

Department of Applied Chemistry,
Faculty of Engineering,
Osaka University
Yamada-oka 2-1, Suita, Osaka 565, Japan
June / 1994

Contents

General Introduction

Semiconductor microcrystals (Q-particles) with diameter less than about 100 Å possess transient properties from bulk materials to molecules due to the size quantization effect and have been very interesting research subjects.[1-9] The size quantization causes splitting the conduction band and valence band into discrete electronic levels in such a way that the potential of the conduction band becomes negative and that of the valence band becomes positive, and the effect becomes remarkable with decreasing the particle size. As an application field of Q-particles in chemistry, the use as photocatalysts have been most intensively studied because the Q-particles have higher reducing and oxidizing powers, as compared to the corresponding bulk materials.

In order to obtain exact information on properties of the Q-particles, it is necessary to prepare particles of rigorously controlled particle size and size distribution, because the electronic structure of the Q-particles depends on their particle size. Various methods for the preparation of Q-particles with a narrow size distribution have been recently developed; immobilization in matrices such as zeolites,[10,11] glasses,[12,13] and polymers,[14,15] the synthesis with use of vesicle[16,17] and surface modifications,[18-28] and biosynthesis.[29] To prepare monodispersed particles, chromatography[30] and electrophoresis[31] have been applied to Q-particles prepared in stabilizing agents. Besides the monodispersity, it is important to characterize surface conditions of Q-particles such as surface charges and surface structures when photocatalytic properties are studied, because Q-particles have a very large surface area compared to their volume which is influenced greatly by stabilizers, solvents and/or solute molecules of electrolyte solutions used in photocatalysis studies.

The chemical modifications of metal sulfide semiconductor microcrystals with use of thiol compounds are reportedly to give a relatively narrow size distribution of the resulting Q-particles. Furthermore, such Q-particles should have more well-defined surface structures than Q-particles prepared with the use of soluble stabilizers and/or

those prepared by immobilization in solid supports such as zeolite and polymer matrices. In this respect it may be said that Q-particles modified with thiol compounds are suitable materials for investigations on the effects of surface conditions on photoinduced charge transfer. While some studies of photoinduced charge transfer with use of the surface-modified Q-particles have been performed, there still remain subjects to be studied; One is to develop effective means for determining the surface structures formed by the bound thiol compounds, and another is to clarify the influence of modified thiol layer on the electron transfer on the Q-particle surface.

The present study has been conducted focusing to clarify the above mentioned subjects of to the surface-modified Q-particles. Furthermore attempts have been made to attach novel functions to Q-particles with use of surface modification methods. Chapter 1 describes a novel method for the analyses of the surface structures of PbS microcrystals modified with 4-hydroxythiophenol and the validity of the analyses is demonstrated by investigations on photoinduced charge transfer from the PbS microcrystals to methylviologen dissolved in solution. Chapter 2 deals with the effects of the surface charges caused by amino groups of the modifier on the photoreduction of methylviologen for PbS microcrystals modified with 4-aminothiophenol. In chapter 3, attachment of abilities of electron mediation to CdS microcrystals using the surface modification with viologen-functionalized thiol is described.

List of Publications

(1) Surface Structure of PbS Microcrystals Modified with 4-Hydroxythiophenol and Their Influences on Photoinduced Charge Transfer

Tsukasa Torimoto, Hiroyuki Uchida, Takao Sakata, Hirotaro Mori, and Hiroshi Yoneyama

J. Am. Chem. Soc. **1993**, *115*, 1874-1880.

(2) Effect of Surface Charge of 4-Aminothiophenol-Modified PbS Microcrystal Photocatalysts on Photoinduced Charge Transfer

Tsukasa Torimoto, Takao Sakata, Hirotaro Mori, and Hiroshi Yoneyama

J. Phys. Chem. **1994**, *99*, 3036-3043.

(3) Preparation of CdS Microcrystals Covalently Bound with Viologen Groups and Their Photoelectrochemical Properties

Tsukasa Torimoto, Kotaro Maeda, Takao Sakata, Hirotaro Mori,

and Hiroshi Yoneyama

Chem. Lett. **1994**, 977-980.

(4) Photoelectrochemical Properties of Size-Quantized CdS Microcrystals Modified with Various Amounts of Viologen-Functionalized Thiol

Tsukasa Torimoto, Kotaro Maeda, Junko Maenaka, and Hiroshi Yoneyama.

J. Phys. Chem. in contribution.

Chapter 1

Surface Structures of PbS Microcrystals Modified with 4-Hydroxythiophenol and Their Influences on Photoinduced Charge Transfer

1-1 Introduction

Synthetic approaches to obtain monodispersed particles with controlled size have been one of the major research interests, and chemical modification by capping with organic reagents seems to be one of the most effective methods to achieve this. For example, thiol and selenol compounds have been successfully used as the capping reagents to prepare quantized CdS, CdSe, CdSe-ZnS, CdSe-ZnSe, and PbS particles[18-28] with narrow size distributions in quantized regime.

Physicochemical properties of these semiconductor microcrystals capped with organic moieties have been studied.[18-28,32-43] In particular, the structure of these particles have been characterized by TEM,[24,25] NMR,[32] X-ray diffraction,[20,25,33] XPS,[34,35] Auger spectroscopy,[34] and EXAFS.[36] However, the characterization of the capped surface in atomic scale has not yet been reported except, for example, using EXAFS, where atomic rearrangements of CdS and CdSe surfaces on capping with benzeneselenol were suggested.

In cases of capped semiconductor microcrystals, it seems very important to clarify the effect of the capping agent on various properties of semiconductor microcrystals, especially in relations to detailed surface structures of capped semiconductors. However, presently no information about this has been reported. So far well-documented results on surface structures, photochemical properties, and photoinduced electron transfers have been obtained only for Cd- and Zn-benzenethiolate clusters,[44-52] which may be regarded as models of monodispersed CdS and ZnS microcrystals.

In this section, I attempt to derive information on the structure of the capped semiconductor surfaces in atomic scale by fitting the experimentally obtained chemical

compositions to those expected from modeled surfaces of capped semiconductors, and the importance of the capped conditions on physicochemical properties of the capped semiconductor microcrystals is demonstrated for 4-hydroxythiophenol-capped PbS microcrystals.

PbS of nanometer size exhibits large quantum size effects due to small effective masses of electrons and holes, and by this reason preparations and photochemical properties of this material including thiol-modified PbS have been studied using various approaches.[15,21,53-58] However, little is known about the relevance of its photochemical properties to the surface structures.

1-2 Experimental Section

All the chemicals used in this study were of reagent grade and purchased from Wako Pure Chemical Industries. Lead acetate trihydrate and sodium sulfide enneahydrate were used as received. Methanol was distilled and 4-hydroxythiophenol (ArSH) was purified by vacuum distillation. Aqueous solutions were prepared using doubly distilled water.

PbS microcrystals capped with ArSH were synthesized by reaction of Pb^{2+} with S^{2-} in the presence of ArSH in methanol at -88 °C. Lead acetate and sodium sulfide were used as the starting materials for Pb^{2+} and S^{2-} ions sources. Lead acetate dissolved in methanol, sodium sulfide dissolved in methanol containing 0.5% water and ArSH dissolved in methanol containing 2.0×10^{-2} M sodium hydroxide were used as the reaction solutions. The concentration of the sulfide was fixed to 5.0×10^{-4} M and that of Pb^{2+} ions and ArSH were varied in such a way that the ratio of $[Pb^{2+}]/[S^{2-}]$ ranged from 1.0 to 6.0 and that of $[ArSH]/[Pb^{2+}]$ from 4.0 to 36.0. A typical procedure for the preparation of ArSH-capped PbS using $[Pb^{2+}]/[S^{2-}]= 3.0$ and $[ArSH]/[Pb^{2+}]= 4.0$ is as follows.

Twenty five milliliters of 3.0×10^{-3} M lead acetate solution was first mixed with 1.2

x 10^{-2} M ArSH solution with an equal volume and cooled at -88 °C with use of dry ice - acetone bath. Then 50 cm^3 of the sodium sulfide solution cooled at -88 °C was added under vigorous stirring. The mixed solution was kept at that temperature for 2 h and then at -20 °C for 1 day, resulting in a transparent brown solution. All the procedures including the preparation of each solution, mixing the solutions, and the reaction at the low temperature were carried out under a stream of N_2.

Absorption spectra of the brown solution were measured at room temperature using a Hewlett-Packard 8452A spectrophotometer after 2-fold dilution. The prepared ArSH-capped PbS microcrystals were observed by a transmission electron microscope (TEM). In order to obtain clear images of ArSH-capped PbS free from any adhered soluble impurities such as Pb^{2+}-ArSH complexes, the brown PbS colloidal solution was concentrated using a 20 Å pore size ultrafilter (Amicon PM-10) under agitation of the solution in the following way. One hundred milliliters of original PbS colloid was filtered until 1 cm^3 of the colloids were left in the cell of the ultrafilter and then 4 cm^3 of deaerated methanol was added to the 1 cm^3 colloid, followed by filtration to leave 1 cm^3 in the cell. The procedures of the addition of 4 cm^3 methanol and the succeeding concentration to 1 cm^3 of the solution using the ultrafilter were repeated until the filtrate showed no appreciable absorption of Pb^{2+}-ArSH complexes. By this procedure, 1 cm^3 of purified PbS colloid was prepared. Then a drop of this colloidal solution was applied to amorphous carbon overlayers on a Cu grid, followed by drying to prepare the TEM samples. High resolution TEM pictures and electron diffraction patterns were obtained at the operation voltage 300 kV (Hitachi, H-9000). During the course of the observations by TEM, however, the microcrystals seemed to be somewhat damaged and aggregated to larger particles. To prevent this undesired event in the determination of the size distribution of PbS microcrystals, observations by TEM under operations with a lower acceleration voltage of 200 kV (Hitachi, H-800) were employed.

To prepare ArSH-capped PbS particles suited for chemical analysis and FT-IR measurement, the purified PbS colloidal solutions were filtered using the ultrafilter, and

the residues on the filter were collected and dried under vacuum. Elemental analysis and atomic absorption spectroscopy were performed using a Yanaco Model MT-2 analyzer and a NJA AA-8500 Mark II spectrometer, respectively. FT-IR spectra were measured by a JASCO FT/IR-3 spectrometer using KBr discs dispersed with the powder of the PbS particles.

For comparative purpose to the ArSH-capped PbS, Pb^{2+}-ArSH complexes were prepared by mixing 3.0×10^{-3} M lead acetate solution with 1.2×10^{-2} M ArSH solution in an equal volume, referring to literatures.[58-60] By evaporating the solvent under vacuum at room temperature, yellow powder was obtained, which was used in FT-IR spectra measurements.

^1H NMR spectra of ArSH-capped PbS particles were obtained in CD_3OD at various temperatures. The preparation of this colloidal solution was made by replacing methanol of the above mentioned purified PbS colloidal solution with CD_3OD. The replacement was carried out by repeating a procedure of the dilution of ArSH-capped PbS colloids with CD_3OD and subsequent filtration of the resulting colloids using the 20 Å ultrafilter to leave a little amount of the concentrated colloidal solution. ^1H NMR spectra were recorded on a JEOL JNM-GSX 400 spectrometer equipped with a cryostat operating at 400 MHz with $Si(CH_3)_4$ internal reference.

Since ArSH-capped PbS colloids were prepared using methanol as the solvent as described above, it is desired to conduct experiments of photoinduced reduction of methylviologen (MV^{2+}) on PbS particles in methanol solutions. However, MV^{2+} is apt to be reduced by methoxide ions.[61] Then photoreduction of MV^{2+} was studied in aqueous solutions. To change the solution environments of ArSH-capped PbS particles from methanol to water, the purified PbS colloids were filtered with the use of the above described ultrafilter and then the wet residue on the filter was put into a deaerated 0.1 M sodium tartrate aqueous solution (pH 7.5). The resulting PbS suspension was subjected to centrifuge. The wet PbS particles obtained were suspended again in the deaerated sodium tartrate solution containing 1.0×10^{-2} M methylviologen dichloride so as to give a

nominal concentration of 2.5 x 10^{-4} M PbS. Sodium tartrate was chosen as a hole scavenger. After bubbling nitrogen for 30 min, the colloid was irradiated with a 500 W Xe lamp through a UV cut-off filter ($\lambda > 400$ nm).

1-3 Results and Discussion

1-3-1 Preparation and Characterization of PbS Microcrystals

In the preparation of the ArSH-capped PbS colloids, the use of very low temperature such as -88 °C seemed essential. If the synthesis was attempted at room temperature, for example, the bulk PbS particles were produced, indicating that the termination of particle growth by ArSH effectively occurs only at very low temperatures where the rate of particle growth is very low in a relative sense.[54,62-64] Once the PbS microcrystalline colloids were prepared, they were stable at room temperature for several months as long as oxygen was excluded from the colloidal solution.

Figure 1-1 shows absorption spectra of PbS microcrystals capped with ArSH, prepared with various concentration ratios of lead ions to sulfide ions which are represented as $[Pb^{2+}]/[S^{2-}]$. All the PbS microcrystals were prepared with excess of ArSH to Pb^{2+} ions, as noticed in the figure caption. A fixed large concentration ratio of $[ArSH]/[S^{2-}]= 36.0$ was adopted in the preparation of all the colloids given in Figure 1-1 to achieve the capping with ArSH as perfect as possible. The synthesis with the use of $[Pb^{2+}]/[S^{2-}]=1.0$ resulted in turbid PbS colloids which contained agglomerated PbS but with $[Pb^{2+}]/[S^{2-}]=1.2$ or the greater, transparent brown PbS colloids were prepared. With increasing the concentration ratio of Pb^{2+} to S^{2-} from 1.2, the absorption onset is blue-shifted, the degree depending on the magnitude of the concentration ratio until the concentration ratio increased to 6.0 and beyond which almost the same absorption spectra were obtained. In addition, it was found that the colloids prepared with the same $[Pb^{2+}]/[S^{2-}]$ ratio gave the same absorption spectra independent of the concentration ratio of $[ArSH]/[Pb^{2+}]$, provided that the $[ArSH]/[Pb^{2+}]$ was equal to or greater than 4.0.

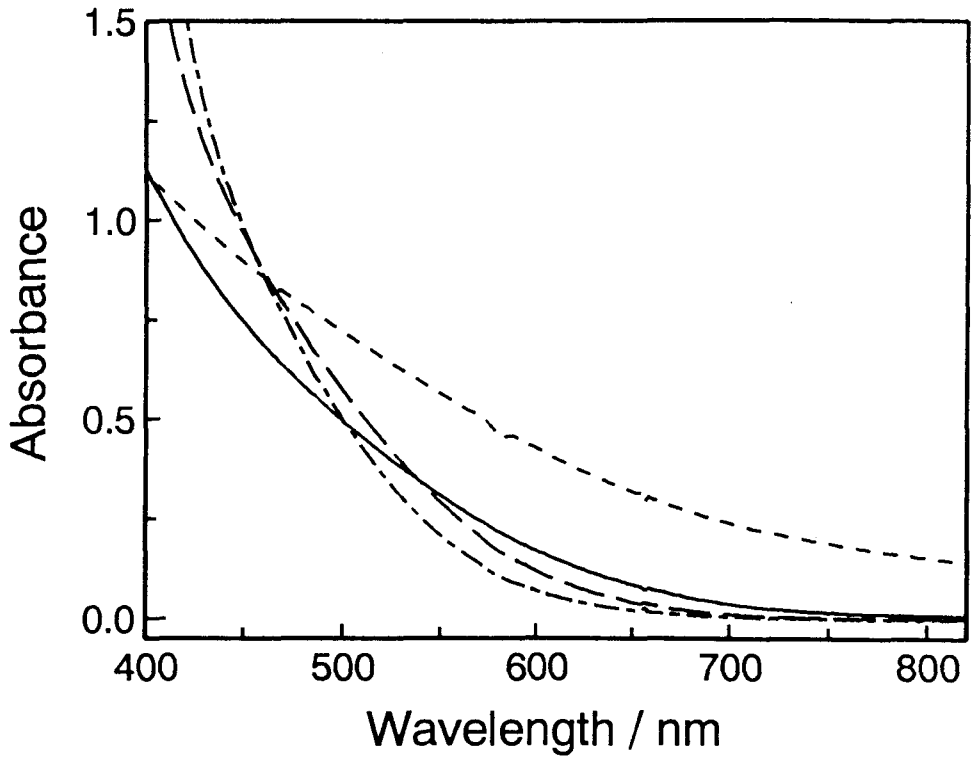

Figure 1-1 Absorption spectra of 1.25×10^{-4} M PbS colloids after dilution with methanol. The molar ratio of $[Pb^{2+}]/[S^{2-}]$:(- - - -) 1.0, (——) 1.2, (- - -) 3.0, (- - -) 6.0. $[S^{2-}]$= 5.0×10^{-4} M and [ArSH]= 1.8×10^{-2} M were fixed in the preparation of all colloids.

A high resolution TEM picture of PbS microcrystals prepared with $[Pb^{2+}]/[S^{2-}]$= 1.2, which is given in Figure 1-2, shows that the particles are almost spherical and have perfect crystallinity of clear periodic lattice planes with no lattice displacement. Electron diffraction patterns of these particles showed that the PbS microcrystals had a rock salt structure.[65] Furthermore, the lattice constant of PbS microcrystals obtained from the TEM picture (Figure 1-2) was 3.43 Å which was in perfect accord with the crystallographic data of the PbS bulk materials. The size distribution of the PbS microcrystals was determined for those prepared with $[Pb^{2+}]/[S^{2-}]$=1.2 and 3.0. In both cases the microcrystals had the same average diameter of 28 Å, but their size distributions were different as shown in Figure 1-3. The standard deviations of 7.4 Å and 4.7 Å were obtained for $[Pb^{2+}]/[S^{2-}]$=1.2 and 3.0, respectively. By applying these results to Figure 1-1, it is recognized that the narrower size distribution gives the steeper rise of absorption spectrum.

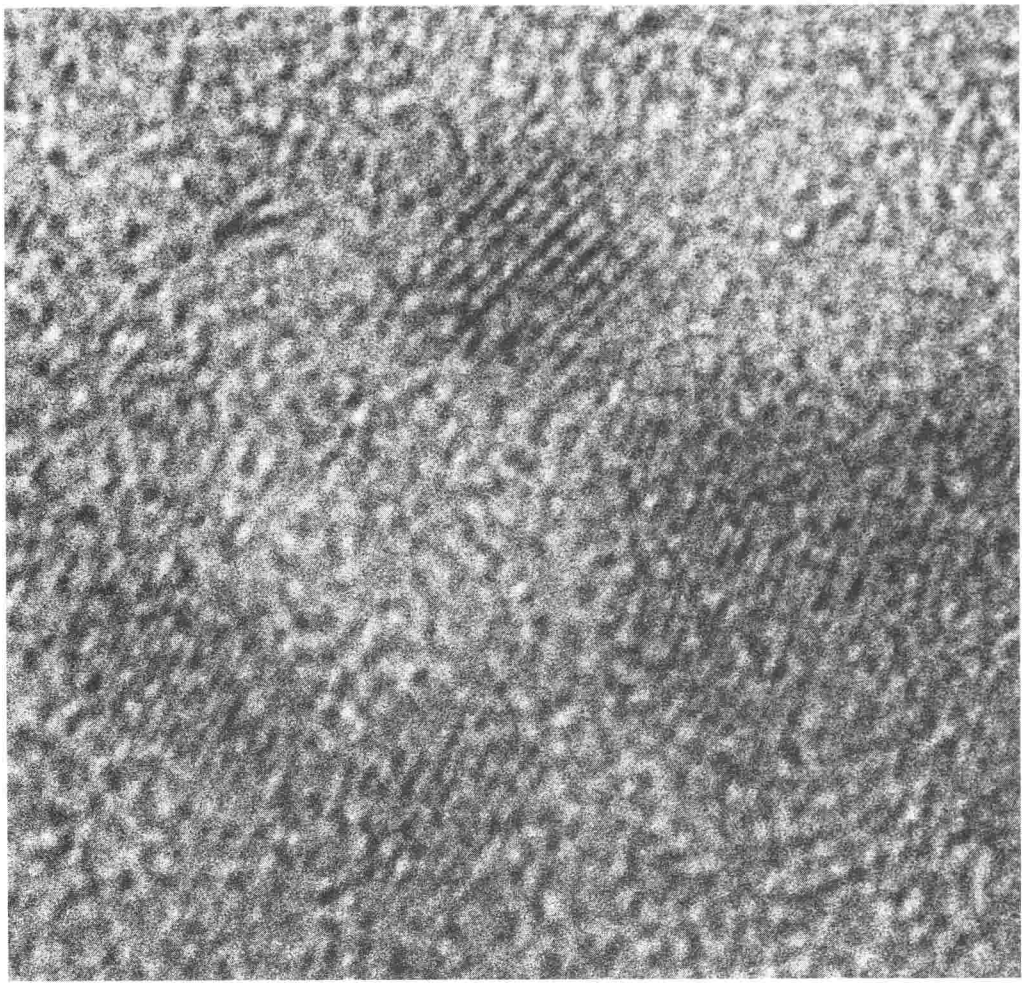

Figure 1-2 High resolution transmission electron micrograph of PbS microcrystals prepared with $[Pb^{2+}]/[S^{2-}]= 1.2$. The lattice spacing is 3.43 Å.

According to Figure 1-1, the PbS colloids prepared with $[Pb^{2+}]/[S^{2-}]=1.2$ has the absorption onset at around 800 nm (1.6 eV) and those prepared with $[Pb^{2+}]/[S^{2-}]=3.0$ at 700 nm (1.8 eV), being much shorter than the absorption threshold of bulk PbS which is 3200 nm.[15]

A theoretical equation to predict the diameter of PbS microcrystals from their energy gaps has been derived by Wang and co-workers.[15]

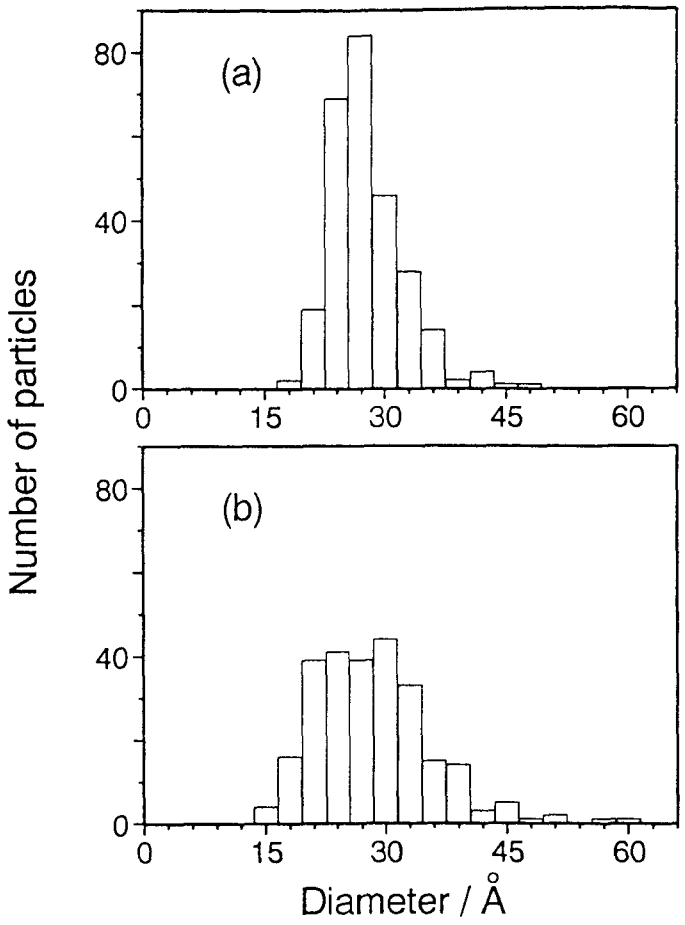

Figure 1-3 Size distributions of PbS microcrystals prepared with $[Pb^{2+}]/[S^{2-}]= 3.0$ (a) and 1.2 (b).

$$E = [E_g^2 + 2E_g (h / 2\pi)^2 (\pi / R)^2 / m^*]^{1/2} \quad (1\text{-}1)$$

$$1 / m^* = (1 / m_e + 1 / m_h) / 2 \quad (1\text{-}2)$$

where E is the energy gap of size quantized PbS, E_g is the band gap of bulk PbS (0.41 eV[66]), R is the particle radius, and m* is given by eq. 1-2, where m_e and m_h are the effective mass of an electron and a positive hole, respectively. By applying the above absorption onset to eq. 1-1 and inserting $m_e = 0.080\ m_o$, and $m_h = 0.075\ m_o$,[66] where m_o is the mass of a free electron, the diameters of PbS microcrystals with $[Pb^{2+}]/[S^{2-}]=1.2$

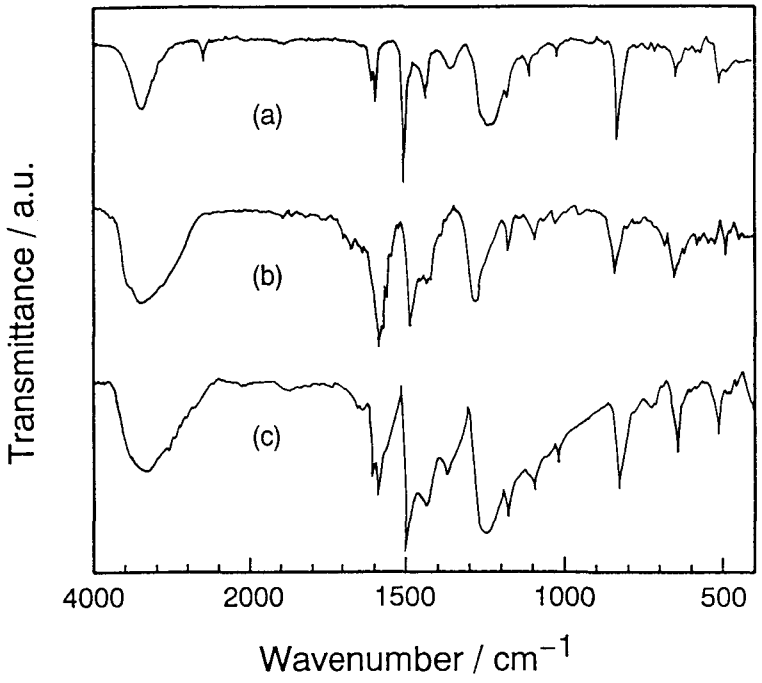

Figure 1-4 FT-IR spectra of 4-hydroxythiophenol (a), Pb^{2+}-ArSH complexes (b) and PbS particles prepared with $[Pb^{2+}]/[S^{2-}]$= 3.0 (c) taken in KBr pellets.

and 3.0 are estimated to be about 39 Å and 33 Å, respectively. These values are in rough accord with the size of the largest PbS particles of relatively high abundance given in Figure 1-3, being consistent with the fact that the absorption onset is determined by the largest particles in colloids.[67]

Figure 1-4 shows a FT-IR spectrum of isolated ArSH-modified PbS particles, that of 4-hydroxythiophenol and Pb^{2+}-ArSH complexes. The absorption peaks assigned to C-C vibrations of a phenyl ring are observed in a range from 1400 to 1600 cm^{-1} and a broad peak around 3300 cm^{-1} is assigned to -OH vibrations. However, an absorption due to -SH vibration observed at 2560 cm^{-1} for pure ArSH is absent both for the PbS particles and for the Pb^{2+}-ArSH complexes, evidencing the achievement of capping Pb^{2+} sites of the PbS microcrystal surfaces with phenyl groups through sulfur atoms of 4-hydroxythiophenol.

^1H NMR spectra of ArSH-capped PbS particles prepared with $[Pb^{2+}]/[S^{2-}]$=3.0 at various temperatures are shown in Figure 1-5. Unfortunately it was unsuccessful to obtain the ^1H NMR spectrum of PbS particles prepared with $[Pb^{2+}]/[S^{2-}]$=1.2, because

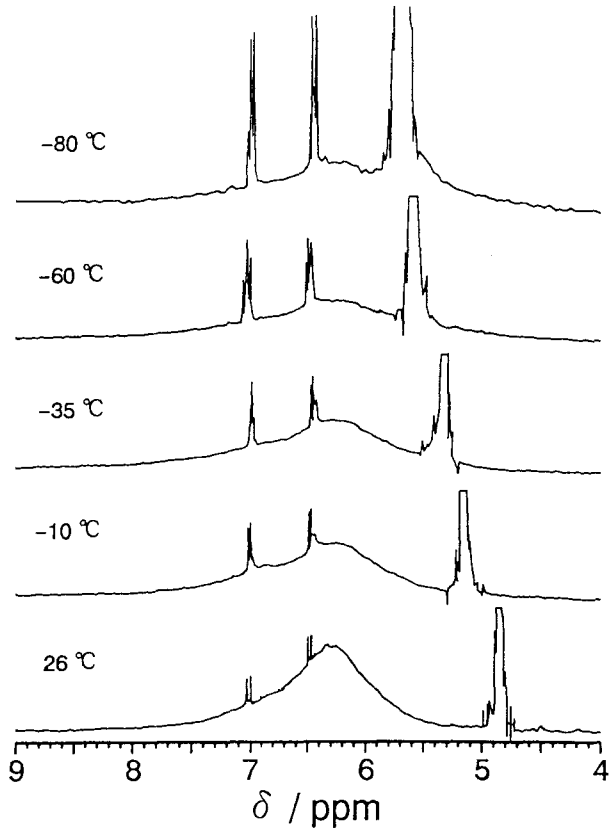

Figure 1-5 ^{1}H-NMR spectra of a ArSH-capped PbS prepared with $[Pb^{2+}]/[S^{2-}]$= 3.0 at various temperatures. The signal intensity is normalized to that of $Si(CH_3)_4$ (not shown).

they were unstable against agglomeration as will be described below in a different section. The resonance of phenyl protons of adsorbed ArSH of PbS particles was splitted into three groups, two of which appeared at 7.02 and 6.47 ppm as sharp signal groups which superimposed on a broad signal peaking at around 6.3 ppm. Sharp signals observed at 4.85 ppm at 26 °C, which shift toward a downfield with lowering temperature, arise from the resonance of the hydroxyl protons of methanol remained in the CD_3OD solution as an impurity. The resonance of phenyl protons of 4-hydroxythiophenol gave only two sharp signals at 7.13 and 6.67 ppm and that of Pb^{2+}-ArSH at 7.11 and 6.56 ppm in CD_3OD, being in a downfield compared to that of PbS particles. It is also found that the intensities of the two sharp signal groups were increased and that of a broad signal peak was decreased with lowering temperatures. The broad signal peak must result from slow

Table 1-1 Analytically Determined Results for PbS Microcrystals Modified with 4-Hydroxythiophenol and Stability Factor against Agglomeration

preparation condition		composition[a]	charge balance[b]	stability factor against agglomeration[c]
$[Pb^{2+}]/[S^{2-}]$	[4-HTP] $/[Pb^{2+}]$	$Pb^{2+}: S^{2-}:HOC_6H_4S^-$		
1.2	4.0	1.30 : 1 : 0.65	1.02	<2
3.0	4.0	1.57 : 1 : 1.56	1.13	>150

[a] Experimentally determined. [b] Calculated by $(2[S^{2-}]+[HOC_6H_4S^-])/(2[Pb^{2+}])$. [c] The factor of concentration at which the PbS colloid began to agglomerate at room temperature, defined as $C_{conc}/C_{original}$, where $C_{original}$ denotes the concentration of PbS present in the original colloids, which were 2.5×10^{-4} M, and C_{conc} denotes that at which the agglomeration began to occur by concentrating the original colloids.

rotation of phenyl groups of the capped ArSH probably with a high density, while the two sharp signal groups are related to phenyl groups in stationary states. With decreasing temperature, the phenyl groups in rotation are decreased, and those in stationary states are increased. Judging from small temperature dependence of the intensity of the broad signal peak, the capped ArSH have wide energy distributions in their rotations.

Results of chemical analyses of the ArSH modified PbS particles are given in Table 1-1 in a relative ratio of Pb^{2+}: S^{2-}: ArS^-. Results obtained for carbon and hydrogen are omitted in this table, because the ratio of these two elements agreed with that expected from the chemical composition of 4-hydroxythiophenolate ions (ArS^-) within experimental error. It is seen that the particles prepared with $[Pb^{2+}]/[S^{2-}] = 3.0$ contained larger fractions of Pb^{2+} and ArS^- than those prepared with $[Pb^{2+}]/[S^{2-}] = 1.2$. A good charge balance is achieved at the particles prepared with $[Pb^{2+}]/[S^{2-}] = 1.2$ as shown in Table 1-1, but the particles prepared with $[Pb^{2+}]/[S^{2-}] = 3.0$ had little excess negative charges that may be compensated by other cations such as protons. The amount of protons used for the charge compensator in such cases, however, are negligible compared to the total amount of hydrogen of ArSH used in capping of PbS microcrystals. Considering that the average size and size distribution of the ArSH-modified PbS

microcrystals are not greatly different between the two kinds of PbS microcrystals, chemical composition should be almost the same unless there is a remarkable difference in the structure of the capped PbS surfaces. Since the chemical analysis results show that there are large differences in the composition between the two kinds of PbS microcrystals, the structure of these capped PbS surfaces must be different.

1-3-2 Surface Structure of the PbS Microcrystals

I have attempted to derive information on the surface structures of the PbS microcrystals in an atomic scale. Three different surface structures as illustrated in Figure 1-6 are first assumed. In this figure, the surfaces are illustrated as plane surfaces but the actual surfaces must be curved, because the prepared microcrystals were spherical, as noticed from Figure 1-2. In these models, I divide a surface region of PbS microcrystals into an adsorbed layer and a core. The core is the particle observed by TEM.

Structure A assumes that S^{2-} sites of the core surfaces are fully occupied by adsorbed Pb^{2+} ions, and both Pb^{2+} sites of the core surfaces and the adsorbed Pb^{2+} are occupied by bound ArS^- to give the complete coverage of PbS microcrystals surfaces with the organic modifier. Structure B assumes that Pb^{2+} sites of the core are completely covered with ArS^- and to compensate excess negative charges due to the bound ArS^- a limited amount of Pb^{2+} ions adsorb on the core surfaces. Structure C is a modification of structure B in the point that ArSH species are bound to the adsorbed Pb^{2+} ions.

1-3-3 Calculation of the Number of Pb^{2+}, S^{2-} and ArS^- in the Capped PbS Microcrystals

The number of Pb^{2+}, S^{2-}, and ArS^- ions constituting PbS microcrystals of different size was calculated for above mentioned structures assuming that all of particles are spherical and have the same rock salt structure. In calculation, a computer was used to

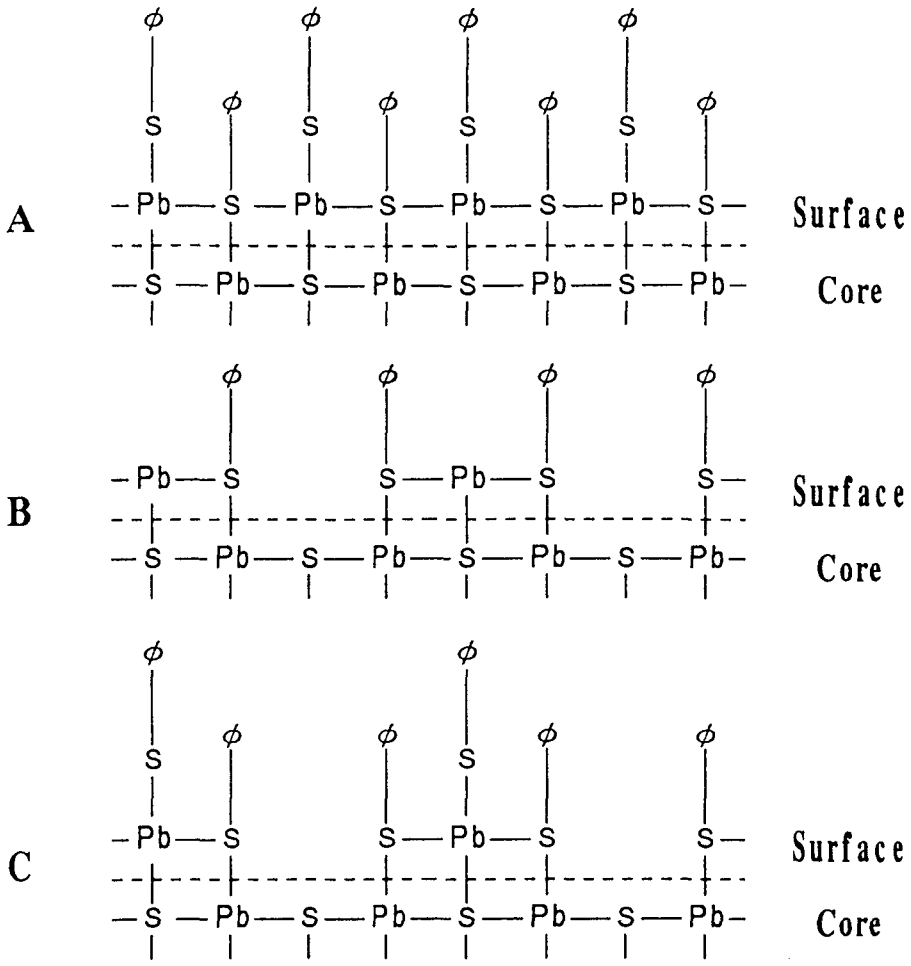

Figure 1-6 Models for surface structures of PbS microcrystals modified with 4-hydroxythiophenol.

count the number of the constituents in building up a particles of a desired size. The procedures of calculations are described below.

Let us consider a sphere having the diameter of d_i in a large PbS single crystal. The atoms constituting the single crystal are divided into two groups with a boundary of the sphere. The atoms present within the sphere constitute a PbS microcrystal core, while those present in adjacent to the sphere surface give adsorbed layers. The atoms which belong to far from the neighborhood of the sphere surface need not be considered here.

The x, y, z axes of coordinates are chosen along with the crystal axes of the PbS rock salt structure. If I choose the center of a spherical particle in such a way that it gives a symmetrical point against the constituent atoms regardless of their kinds, I have four different centers P_j (p, q, r) which are given by eq. 1-3 ($p, q, r \geq 0$).

$$P_1(0, 0, 0),\ P_2(\alpha/2, 0, 0),\ P_3(\alpha/2, \alpha/2, 0),\ P_4(\alpha/2, \alpha/2, \alpha/2) \qquad (1\text{-}3)$$

$$\alpha = a_0/2 \qquad (1\text{-}4)$$

where a_0 is the lattice constant of the PbS rock salt structure and equal to 5.9362 Å.[65] It is necessary to specify an atom of interest (X) in the single crystal whether it is Pb or S. If an atom X is given by $(l\alpha, m\alpha, n\alpha)$, where l, m and n are integral numbers, the kinds of atoms must be discriminated by the value of $(l + m + n)$. If the odd number is chosen for Pb, then S is for the even number. The reverse is also true. Calculations described below were made for both cases of the presence of Pb^{2+} ion on the origin ($l = m = n = 0$) and of S^{2-} ion on the origin. If I had a little different numbers of atoms between the two kinds of calculations, the numbers were averaged.

If the closest distance (P_jX) between the atom X and the center of the sphere is smaller than the radius of the sphere, that is, P_jX fulfills the condition given by eqs. 1-5 and 1-6, then I find that the atom is included in a PbS microcrystal core of a diameter d_i.

$$P_jX = \{ (p - l\alpha)^2 + (q - m\alpha)^2 + (r - n\alpha)^2 \}^{1/2} \qquad (1\text{-}5)$$

$$P_jX < d_i/2 \qquad (1\text{-}6)$$

In this way, calculations were made for P_jX great enough to cover $d_i/2$. The atoms of Pb and S included in a core having the diameter d_i are selected and the number of them is counted for every P_j ($j = 1 \sim 4$). Different P_j gives a little different number of total

atoms included in a core of the same diameter d_i. I have chosen the largest number (V_{max}) obtained among the four kinds of P_j. The P_j that gives V_{max} is denoted here as P_{max}. Even if the equation " $P_jX \leq d_i/2$ " is used instead of eq. 1-6 to include atoms on the border of the particle, calculations show that the contribution of the border is minor.

If the atom X is present outside the sphere but is bound to at least one atom of the microcrystal core surface, it is counted as the atom involved in the construction of the adsorbed layer. The adsorbed layer of this kind is denoted here as the first adsorbed layer. If the atom X is present outside the first adsorbed layer in such a way that it is bound to at least an atom of the first adsorbed layer, it is counted as the atom involved in the construction of the second adsorbed layer. As far as the surface structure models proposed in Figure 1-6 are concerned, it is enough to take into consideration of the PbS core and the first and the second adsorbed layers. Accordingly if an atom X satisfies eqs. 1-7, 1-8 and 1-9 with use of above determined $P_{max}(p, q, r)$, then it is counted as the atom in the adsorbed layers.

$$P_{max}X \geq d_i/2 \tag{1-7}$$

$$\{p - (l + \Delta l)\alpha\}^2 + \{q - (m + \Delta m)\alpha\}^2 + \{r - (n + \Delta n)\alpha\}^2 < (d_i/2)^2 \tag{1-8}$$

$$|\Delta l| + |\Delta m| + |\Delta n| = k, \quad k = 1, 2 \tag{1-9}$$

In eq. 1-9, $k = 1$ and $k = 2$ represent the situation that the atom X exists in the first and second adsorbed layer above surface core atoms, respectively.

Calculation of the number of Pb^{2+}, S^{2-} and ArS^- in a ArSH-capped PbS particle was made by using these procedures. The number of the Pb and S atoms determined in this way, however, does not directly give information of the surface structures. What is necessary to be done is to modify the number of Pb and S atoms obtained for the adsorbed layers to that of the respective surface structures. For example, in the case of a Q-PbS

particle having structure A, the number of Pb^{2+} ions in the second adsorbed layer must be subtracted from the total number of Pb^{2+} ions in the adsorbed layers. Since S atoms obtained for the adsorbed layers are those originated from the thiol compound, PbS particles having structure A have Pb^{2+} ions and ArS^- ions in the first adsorbed layer and ArS^- ions in the second adsorbed layer. By summing up the number of these constituents and the number of Pb^{2+} and S^{2-} ions of the PbS particle core having the diameter d_i, I can have a theoretical composition of Pb^{2+}, S^{2-} and ArS^- for this particle. As for structure B, the second layer is omitted, and since the number of Pb^{2+} ions that are required to compensate negative charges of ArS^- ions in the first adsorbed layer is one-half the number of the ArS^- ions, this number is adopted as the number of Pb^{2+} ions for the adsorbed layer of the PbS particle. By summing up the number of Pb^{2+} ions and ArS^- ions in the adsorbed layer and the number of Pb^{2+} and S^{2-} ions constituting the PbS core, I can have a composition of Pb^{2+}, S^{2-} and ArS^- for a Q-PbS particle with the diameter d_i whose surface structure is that given by structure B on average. The theoretical composition of a Q-PbS particle having structure C can be obtained in a similar way. The results are given in Table 1-2.

1-3-4 Structure of PbS Microcrystals Modified with 4-Hydroxythiophenol

By taking the size distributions given in Figure 1-3 into account, the average number ($<N_x>$) of Pb^{2+}, S^{2-} and ArS^- of a PbS particle, defined by eq. 1-10, was obtained for particles prepared with $[Pb^{2+}]/[S^{2-}]$=1.2 and 3.0

$$<N_x> = \sum_i N_x F(d_i) \qquad (1\text{-}10)$$

where $F(d_i)$ is a fraction of PbS microcrystals with a diameter d_i in the colloids and N_x is the number of the constituent (x = Pb^{2+}, S^{2-} or ArS^-) of a particle of the same radius having structure A, B or C, which are listed in Table 1-2. The results are given in Table 1-3.

Table 1-2 Number of Pb^{2+}, S^{2-} and ArS^- Constituting a Particle of Various Diameters Having Structure A, B and C, and the Experimentally Determined Size Fraction

diameter	structure A			structure B			structure C			size fraction $[Pb^{2+}]/[S^{2-}]$[a]	
(Å)	Pb^{2+}	S^{2-}	ArS^-	Pb^{2+}	S^{2-}	ArS^-	Pb^{2+}	S^{2-}	ArS^-	1.2	3.0
9	31	10	58	21	10	21	21	10	40	0	0
12	48	18	78	33	18	30	33	18	54	0	0
15	86	41	112	63	41	45	63	41	79	0.016	0
18	128	68	144	98	68	60	98	68	102	0.062	0.007
21	182	98	198	140	98	84	140	98	141	0.151	0.070
24	249	144	242	197	144	105	197	144	174	0.159	0.256
27	326	201	286	264	201	125	264	201	206	0.151	0.311
30	434	277	354	356	277	157	356	277	255	0.171	0.170
33	547	370	396	458	370	177	458	370	287	0.128	0.104
36	700	484	480	592	484	216	592	484	348	0.058	0.052
39	860	607	556	733	607	253	733	607	405	0.054	0.007
42	1043	752	636	897	752	291	897	752	464	0.011	0.015
45	1256	928	712	1092	928	328	1092	928	520	0.019	0.004
48	1508	1136	804	1322	1136	372	1322	1136	588	0.004	0.004
51	1754	1340	890	1547	1340	414	1547	1340	652	0.008	0
54	2052	1592	988	1822	1592	460	1822	1592	724	0	0
57	2385	1872	1096	2128	1872	513	2128	1872	805	0.004	0
60	2776	2193	1240	2484	2193	583	2484	2193	912	0.004	0
63	3160	2528	1342	2844	2528	632	2844	2528	987	0	0
66	3592	2916	1432	3254	2916	676	3254	2916	1054	0	0
69	4108	3352	1596	3730	3352	756	3730	3352	1176	0	0
72	4600	3784	1720	4192	3784	816	4192	3784	1268	0	0

[a] Experimentally obtained size fraction of PbS particles calculated from Figure 1-3

It is seen that differences in the surface structure are reflected more clearly in the composition of ArSH-capped PbS microcrystals rather than in the charge balance. This implies that experimentally determined compositions can be used as a diagnostic criteria to deduce the surface structure of prepared ArSH-capped PbS. It is not unreasonable to think that there are many different surfaces in a prepared ArSH-capped PbS microcrystal as already discussed above on ^1H NMR spectra of the capped ArSH, but, by comparing the experimentally determined compositions with those given in Table 1-3, I can derive information on what surface structure is predominant in the prepared microcrystals. It is found from comparison of the calculated values with analytically determined results that

Table 1-3 Analytically Determined Compositions and Theoretical Compositions Given by Structure A, B and C.

$[Pb^{2+}]$ /$[S^{2-}]$		component[a]			relative composition	charge balance
		Pb^{2+}	S^{2-}	ArS^-	Pb^{2+} : S^{2-} : ArS^-	
1.2	anal.[b]				1.30 : 1 : 0.65	1.02
	structure A	433	286	332	1.51 : 1 : 1.16	1.04
	structure B	359	286	147	1.26 : 1 : 0.51	1.00
	structure C	359	286	239	1.26 : 1 : 0.84	1.13
3.0	anal.[b]				1.57 : 1 : 1.56	1.13
	structure A	378	241	311	1.57 : 1 : 1.29	1.05
	structure B	309	241	137	1.29 : 1 : 0.57	1.00
	structure C	309	241	224	1.29 : 1 : 0.93	1.14

[a]The number of each component containing of a PbS particle having the average diameter, calculatedby eq. 1-20. [b]Analytically determined results given in Table 1-1.

the composition of the PbS particles prepared with $[Pb^{2+}]/[S^{2-}]=1.2$ is in excellent agreement with that predicted by structure B and that of the particles prepared with $[Pb^{2+}]/[S^{2-}]=3.0$ is fitted to structure A, although a little deficiency of ArS^- is noticed for analytically determined result.

At this stage it seems important to discuss the validity of the proposed surface structures. It is suggested from considerations based on the molecular size of the capped ArSH that the proposed surface structures are impractical for bulk single crystals due to steric hindrance of the phenyl groups of the capped ArSH. However, the problem of steric hindrance is relaxed with decreasing the particle size, because the capping of ArSH occurs on a convex surface of the particles and the degree of the curvature is higher for smaller particles. The critical diameter of ArSH-capped PbS particle having such structures is roughly estimated in the following way.

The number of the capped ArSH on the core surface of a PbS particle of the diameter d_i is not greater than that obtained by dividing the surface area of the capped PbS particle by the cross section of the phenyl group. This threshold number is represented here as N_{max}, which is given by eq. 1-11

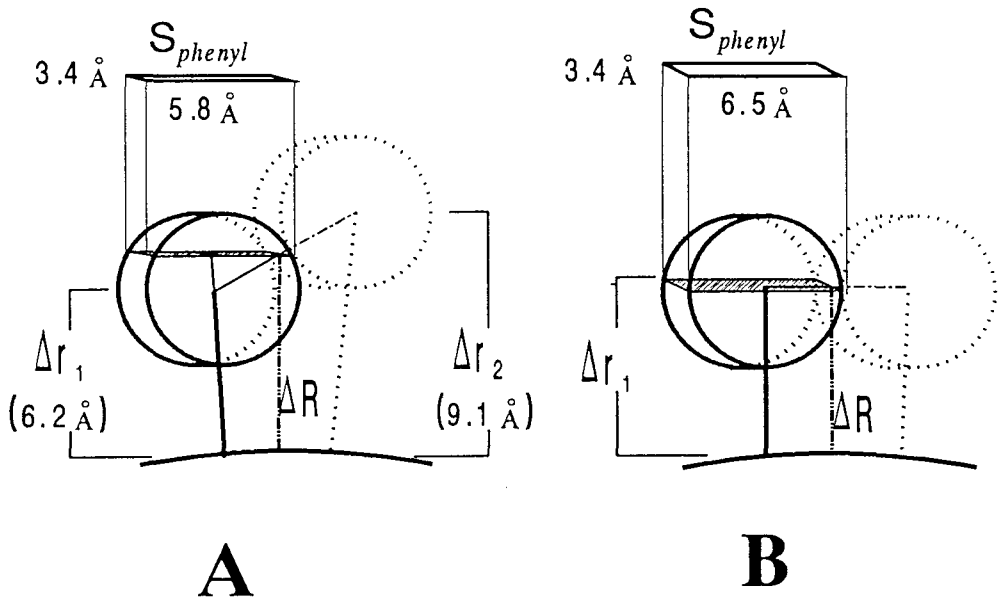

Figure 1-7 Geometrical configurations of the capped ArSH for Structure A and B.

$$N_{max} = 4\pi (\Delta R + d_i/2)^2 / S_{phenyl} \qquad (1\text{-}11)$$

where ΔR is the distance from the surface of the PbS core to the point where a capped phenyl group comes in contact with an adjacent one, and S_{phenyl} is the cross section of the phenyl group at the distance ΔR (see Figure 1-7). In the following calculation, the values of 3.0, 1.8, and 1.4 Å are used as the bond length of Pb-S, S-C, and C-C,[60,65,68] and a phenyl group is assumed to be a disk of 6.5 Å diameter and 3.4 Å thickness which was estimated based on the crystal structure of benzene and van der Waals radius of a carbon atom.[69,70]

If the 4-hydroxythiophenolate ions are linearly bound to Pb atoms of the core surfaces and to the Pb^{2+} ions adsorbed on S atoms in the core surface, then 6.2 Å (= Δr_1) and 9.1 Å (= Δr_2) are obtained, respectively, for distances between the centers of the bound phenyl groups and the surface of the PbS core as illustrated in Figure 1-7. S_{phenyl}

for that structure is calculated to be 19.6 $Å^2$ by using Δr_1, Δr_2 and the diameter of phenyl groups, and ΔR is an average value (7.7 Å) of Δr_1 and Δr_2. In the cases in which all of the ArS^- ions are bound to Pb sites of the core surfaces as in structure B, the phenyl groups make contacts with each other at the distance Δr_1 from the PbS core surface as also illustrated in Figure 1-7. Then, ΔR is equal to Δr_1 and S_{phenyl} is calculated to be 22.1 $Å^2$.

The largest particles that were experimentally obtained for structure B were those having the diameter of 60 Å. By inserting this value together with ΔR and S_{phenyl} into eq. 1-11, I have N_{max}= 745, which is much greater than the number of capped ArSH given in Table 1-2 for structure B. Thus structure B is practical. In the case of structure A, I have a serious geometrical restriction. By inserting the above described ΔR and S_{phenyl} values into eq. 1-11 for a variety of d_i, it is found that PbS particles having the diameter equal to or smaller than 27 Å give N_{max} greater than the number of ArSH given in Table 1-2. Accordingly structure A is practical for particles having the diameter less than 27Å.

According to results shown in Figure 1-3, the largest particle experimentally obtained with high abundance for $[Pb^{2+}]/[S^{2-}]$=3.0 had the diameter of 33 Å, being greater the largest limit described above from the geometrical consideration for Structure A. However, if N_{max} of eq. 1-11 is calculated for a particle of 33 Å, it is found that N_{max} of about 6 % less than that given in Table 1-3 is obtained. Therefore it seems reasonable to conclude that structure A is predominant in the particles prepared with $[Pb^{2+}]/[S^{2-}]$=3.0.

Recently, EXAFS studies[36] on phenyl-capped CdSe and CdS have revealed that the crystallographic structures of CdS and CdSe microcrystal surfaces are deformed by capping with benzenethiol and benzeneselenol. If similar things happened in the ArSH-capped PbS, perfect coincidence of the experimental results with the calculated results would not be anticipated.

1-3-5 Stability to Agglomeration

According to the above identification of the surface structures of ArSH-capped PbS, the PbS particles prepared with $[Pb^{2+}]/[S^{2-}]= 1.2$ have partially unmodified surface sites that allow contacts with solution, and they have no net charge in the surfaces. In contrast those prepared with $[Pb^{2+}]/[S^{2-}]= 3.0$ are almost completely covered with ArSH and have negative charges on the surface. Then it is expected that the latter colloid is stable against agglomeration as compared to the former colloid, because of the presence of negative surface charges and of more hydroxyl groups of organic modifier than the former. The hydroxyl groups assist in solvation with polar solvents, making the microcrystal stable. Such expectation was demonstrated in the following experiments.

When 100 cm^3 of the transparent brown PbS original colloid ($[PbS]= 2.5 \times 10^{-4}$ M) prepared with $[Pb^{2+}]/[S^{2-}]= 1.2$ was filtered using the ultrafilter (pore size 20 Å) under agitation, the colloid become turbid at the time when about one-half of that colloid solution was filtered, while the colloidal solutions prepared with $[Pb^{2+}]/[S^{2-}]= 3.0$ kept its brown transparency even when the colloid was concentrated to 1/150 (Table 1-1).

1-3-6 Photoreduction of Methylviologen

PbS microcrystals of 30 Å or the less have potentials negative enough to reduce methylviologen[21,56] whose redox potential is -0.45 V vs NHE.[71] PbS microcrystals prepared in the present study should have capabilities for reducing methylviologen, as judged from the size quantization based on their particle size.

As expected, irradiation with a 500W Xe lamp of the ArSH capped PbS suspensions containing methylviologen (MV^{2+}) in the presence of sodium tartrate as a hole scavenger resulted in methylviologen radical cations ($MV^{\bullet +}$), which were recognized from the characteristic absorption peaks of $MV^{\bullet +}$ at 396 nm and 606 nm[72] both of which superimposed on the absorption spectrum of the PbS colloid. During the course of the

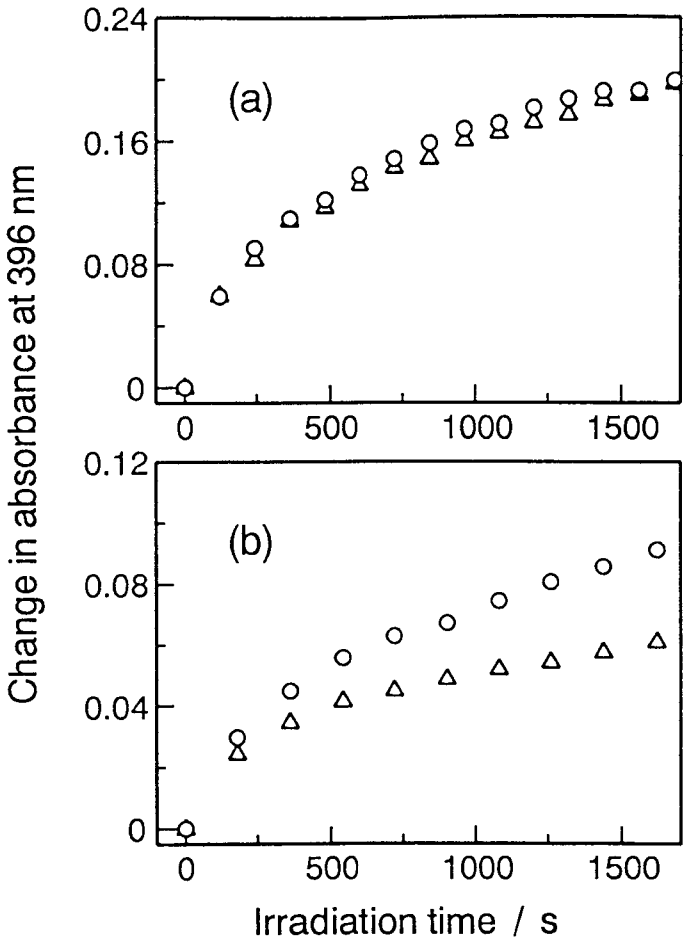

Figure 1-8 Time course of changes in absorbance at 396 nm caused by photoreduction of MV^{2+}. (a) PbS colloids prepared with $[Pb^{2+}]/[S^{2-}]= 3.0$ and (b) those prepared with $[Pb^{2+}]/[S^{2-}]= 1.2$. 2.5×10^{-4} M PbS colloids contained 1.0×10^{-2}M MV^{2+} and 0.1M sodium tartrate and its pH was 7.5: (○) original suspension and (△) with addition of 5.0×10^{-5} M Pb^{2+} ; light source ; 500 W Xe lamp ($\lambda > 400$ nm).

irradiation, the absorption spectra of the two kinds of PbS colloids prepared with $[Pb^{2+}]/[S^{2-}]= 1.2$ and 3.0 were not changed at all, suggesting that the PbS microcrystals were not photocorroded.

Figure 1-8 shows the time course of changes in absorbance at 396 nm caused by photoinduced formation of $MV^{\bullet+}$. It was found that the rate of $MV^{\bullet+}$ production was remarkably hindered by the addition of 5.0×10^{-5} M $Pb(CH_3COO)_2$ for the PbS colloids prepared with $[Pb^{2+}]/[S^{2-}]= 1.2$, as shown in Figure 1-8(b), while little effect of the addition of Pb^{2+} ions was noticed for the PbS colloids prepared with $[Pb^{2+}]/[S^{2-}]= 3.0$

(Figure 1-8(a)). As already discussed above, the former PbS has unmodified surface sites (sulfur sites) on which Pb^{2+} ions can adsorb. If the adsorbed Pb^{2+} scavenges a fraction of photoexcited electrons, the rate of reduction of methylviologen must be decreased, as observed. In contrast, the adsorption of Pb^{2+} ions must occur with less extent for the PbS particles prepared with $[Pb^{2+}]/[S^{2-}]= 3.0$, because surface sites of the particles are fully occupied by ArS^-.

It has been reported that PbS microcrystals modified with 3-mercapto-1,2-propanediol emit a strong fluorescence in a visible region.[21] However, this was not observed for the ArSH modified PbS microcrystals prepared in this study. Accordingly it is speculated that ArS^- groups bound to the PbS microcrystals surfaces quench the fluorescence. The capped ArSH may transfer its electrons to photogenerated holes in PbS microcrystals. It was found that MV^{2+} was photoreduced in the ArSH-capped PbS in the presence of tartrate as a hole scavenger. However, the photoreduction did not take place in the absence of tartrate. These findings seem to suggest that in the absence of tartrate, the capped-ArSH is oxidized by the valence band holes and the oxidized ArSH accepts photogenerated electrons from the conduction band, giving no chance for photoreduction of MV^{2+}. If this were the case, then the capped ArSH might work as a mediator for oxidation of some chemical species in solution.

1-4 Conclusion

By changing the relative concentration of Pb^{2+} ions to S^{2-} ions in the synthesis of PbS microcrystals with a fixed $[ArSH]/[Pb^{2+}]$ ratio of 4.0, different structures of the capped surfaces were prepared. The most important discovery in the present study is that such difference in the surface structures greatly effects photochemical and photoelectrochemical properties of the capped PbS microcrystals. Furthermore a suggestion was obtained that the surface organic groups, the capped ArSH, have capabilities of the mediation in the electron transfer reactions.

Chapter 2

The Effect of Surface Charge of 4-Aminothiophenol-Modified PbS Microcrystal Photocatalysts on Photoinduced Charge Transfer

2-1 Introduction

In the past decade, photoinduced charge transfers on size-quantized semiconductor particles (Q-particles) have been fairly intensively investigated using redox agents of high reversibilities such as methylviologen[73-81] and SCN^-.[73,82,83] To have exact information on charge transfer events on Q-particles, it seems important to clarify the effect of surface conditions on the charge transfers, because the interfacial charge transfer occurs at the semiconductor surface / liquid electrolyte interfaces, which is believed to be influenced more or less by surface conditions of photocatalysts. The term of surface conditions used here includes surface charges and chemical compositions. Certainly it has been reported that the photoinduced charge transfer from Q-particles to redox species in the solution phase was influenced by the surface charges of Q-particles.[77,84-91] In chapter 1, I have recently reported for the photoreduction of MV^{2+} on 4-hydroxythiophenol-modified Q-PbS particles that the degree of the surface modification influenced greatly the rate of photoinduced reduction of methylviologen. However, little is known about the details.

As related subjects to the photoinduced charge transfers on thiol-modified Q-particles, several electron transfer reactions have been investigated at self-assembled thiol monolayer films on gold electrode.[94-104] In the case of 4-aminothiophenol(4-ATP)-modified Au electrodes in aqueous electrolyte solutions,[103] the electron transfer to anthraquinone- 2,6-disulfonate is influenced by the pH of the electrolyte solutions due to variations of charged conditions of the modified layer.

With the surface modification, new and/or novel functions are attached to Q-particles as demonstrated, for example, in Q-CdS modified with thiol

compounds.[35,92,93] Recently it has been reported that photoinduced charge transfers on Q-CdS particles modified with mercaptoethylamine were influenced by the introduced functional groups on the surface.[92,93] By the modification with 4-ATP of Q-PbS particles, therefore, pH-sensitive particle surfaces can be prepared. In this section, the effects of surface charges on the rate of photoreduction of methylviologen with use of 4-ATP-modified Q-PbS particles are described with focusing to the degree of the 4-ATP coating and the role of both hole scavengers and inert electrolyte ions used.

2-2 Experimental Section

4-Aminothiophenol (4-ATP) was obtained from Aldrich and purified by vacuum sublimation prior to use. Methylviologen dichloride of reagent grade purchased from Tokyo Chemical Ind. was used as received. Other chemicals used in this study were of reagent grade and purchased from Wako Pure Chemical Ind. Methanol was distilled, and aqueous solutions were prepared using doubly distilled water.

PbS microcrystals capped with 4-ATP, which is denoted in this section as 4-ATP/Q-PbS, were synthesized by using the same procedures as those described in chapter 1. In these procedures, the concentration of sodium sulfide was fixed to 5.0×10^{-4} M, and the concentration ratio of $[4\text{-ATP}]/[Pb^{2+}]$ was fixed to 4.0, but that of $[Pb^{2+}]/[S^{2-}]$ was varied to either 1.2 or 1.6.

The 4-ATP/Q-PbS suspensions were subjected to centrifuge to isolate the particles, and the wet PbS particles obtained were suspended again in deaerated methanol. The procedure of the centrifuge and suspending was repeated several times until a supernatant did not show any appreciable absorbance characteristics of Pb^{2+}-4-ATP complexes. The purified suspensions in methanol prepared in this way were used for TEM and chemical analyses.

For investigations on the charge transfer and the measurements of potentiometric titration, the methanol solvent of the purified 4-ATP/Q-PbS suspension was replaced by

distilled water. By application of the centrifuge, the wet PbS particles were obtained, which were suspended in distilled water. The resulting suspension was again centrifuged, and the obtained wet 4-ATP/Q-PbS particles were suspended in distilled water.

The samples for TEM and electron diffraction analyses were prepared by dropping the 4-ATP/Q-PbS suspension onto amorphous carbon overlayers on a Cu grid, followed by drying. A Hitachi H-800 transmission electron microscope at operation voltage of 200 kV was used for these measurements.

For chemical analyses, the 4-ATP/Q-PbS particles were isolated from the purified suspensions and dried under vacuum. To determine the composition of the 4-ATP/Q-PbS particles, weight fractions of C, H, N, and S of the particles were determined by elemental analyses and that of Pb by atomic absorption spectroscopy. Elemental analyses and atomic absorption spectroscopy were performed using a Yanaco Model MT-2 analyzer and an NJA AA-8500 Mark II spectrophotometer, respectively. The molar ratio of C, H and N obtained was equal to that expected from the chemical formula of $NH_2C_6H_4S^-$ within experimental errors, and then the amount of $NH_2C_6H_4S^-$ was straightforwardly determined. By subtraction of the amount of S used as the component of $NH_2C_6H_4S^-$, the amount of S^{2-} ions in the PbS particles were determined. Then the relative ratio of Pb^{2+} : S^{2-} : $NH_2C_6H_4S^-$ was obtained.

The 4-ATP/Q-PbS particles (2.5×10^{-3} M) suspended in 10 cm^3 of 1.0×10^{-3} M NaOH aqueous solution were titrated with 1.0×10^{-3} M $HClO_4$ aqueous solution under N_2 atmosphere. Both NaOH and $HClO_4$ solutions contained 1.0×10^{-2} M $NaClO_4$ as a supporting electrolyte and were prepared under N_2 atmosphere to avoid CO_2 inclusion. The pH of the suspensions were measured using a Horiba pH meter F-13 during the course of titrations.

Photoreduction of methylviologen (MV^{2+}) on the 4-ATP/Q-PbS particles was studied using a solution that contained 1.0×10^{-3} M MV^{2+} as an electron acceptor, 0.1 M sodium tartrate or triethanolamine (TEOA) as a hole scavenger and 2.0×10^{-4} M 4-ATP/ Q-PbS particles. This solution (4 cm^3) was put in an optical quartz cell (1 cm x 1 cm x 4

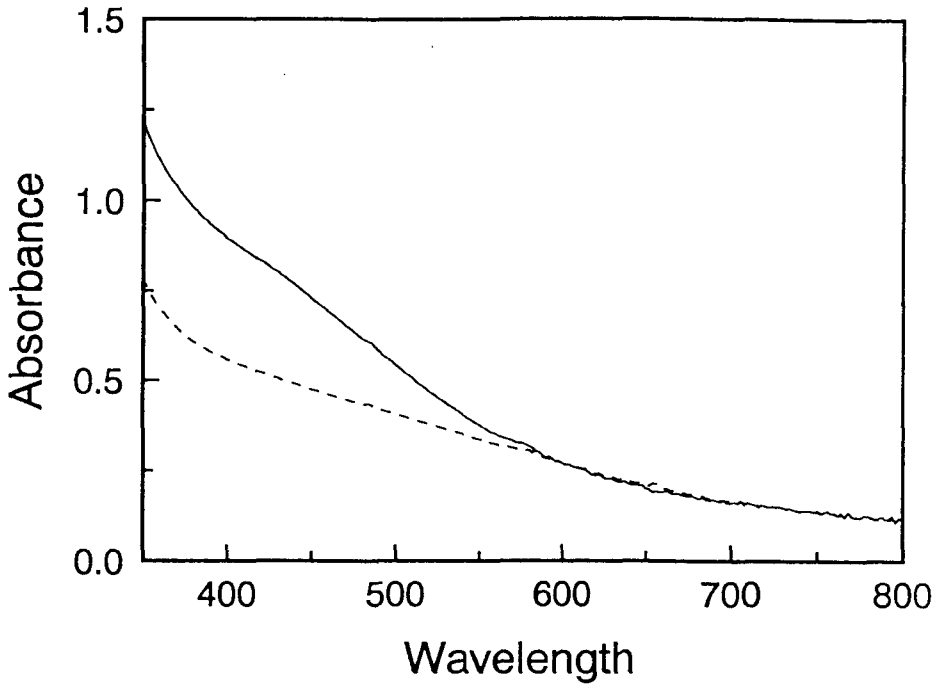

Figure 2-1 Absorption spectra of methanol suspensions containing 5.0 x 10^{-5} M 4-ATP/Q-PbS. The prepared conditions of the 4-ATP/Q-PbS particles: $[Pb^{2+}]/[S^{2-}]$= 1.6 (——) and 1.2 (- - - -).

cm height), evacuated to remove dissolved O_2 and finally filled with N_2. Then the solution was irradiated with a 500 W Xe lamp through UV cutoff (λ< 400 nm) and IR cutoff filters. The adjustment of the pH of the solutions was made by NaOH or $HClO_4$, but for cases where other electrolytes were intentionally added to the solutions, the pH adjustment was made by using acid that had the same anion as the electrolyte.

The quantum efficiency for the initial formation rate of methylviologen radical cation was obtained using a solution that contained 2.0 x 10^{-4} M 4-ATP/Q-PbS particles prepared with $[Pb^{2+}]/[S^{2-}]$= 1.6, 1.0 x 10^{-3} M MV^{2+} and 0.1 M tartrate. The solution pH in that case was adjusted by HCl to pH 5.0. Irradiation was performed with the 500 W Xe lamp through a 410 nm interference filter. The number of incident photons was measured using a thermopile, Eppley lab. Model E-6.

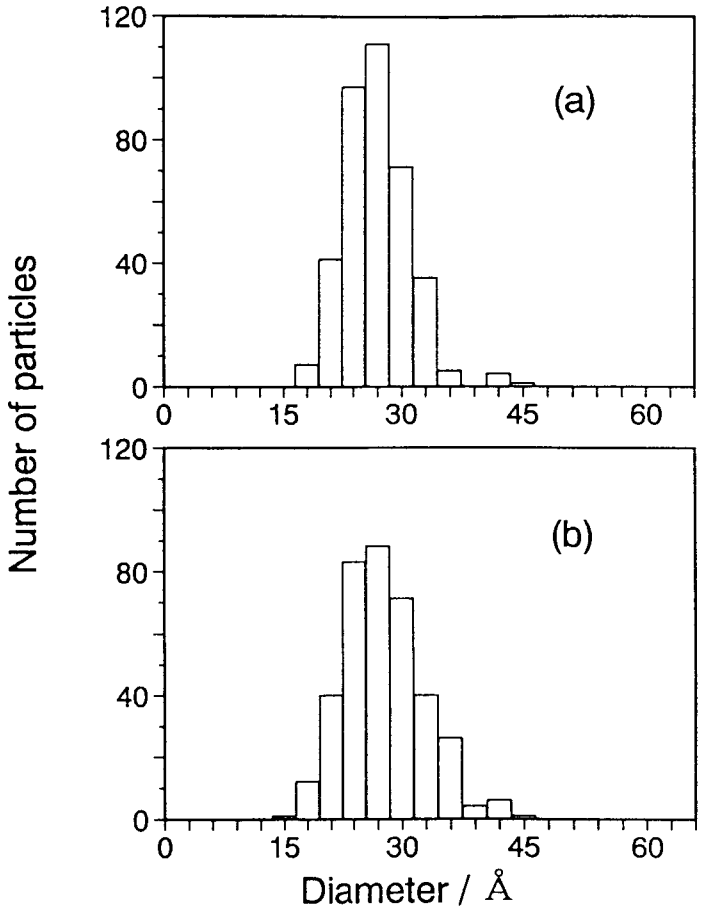

Figure 2-2 Size distribution of the 4-ATP/Q-PbS particles prepared with $[Pb^{2+}]/[S^{2-}]= 1.6$ (a) and 1.2 (b).

2-2 Results and Discussion

2-2-1 Preparation and Characterization of PbS Microcrystals

Figure 2-1 shows absorption spectra of two kinds of the 4-ATP/Q-PbS particles. One was prepared with the concentration ratio of $[Pb^{2+}]/[S^{2-}]= 1.2$ and the other with 1.6. Both show the absorption threshold at about 600 ~ 700 nm, which is not exactly resolved but is much shorter than the threshold of bulk PbS,[15] indicating the large quantum size effects. Unfortunately, the 4-ATP/Q-PbS particles could not be dissolved in both methanol and water, and then suspensions were used in the present study.

According to observations by TEM, the particles were spherical, and they had size

Table 2-1 Analytically Determined Results for PbS Microcrystals Modified with 4-ATP

$[Pb^{2+}]/[S^{2-}]$			$Pb^{2+}: S^{2-}: NH_2C_6H_4S^-$ composition
1.2		anal.[a]	1.20 : 1 : 0.64
	theor calcn	structure A	1.57 : 1 : 1.29
		structure B	1.28 : 1 : 0.57
		structure C	1.28 : 1 : 0.93
1.6		anal.[a]	1.59 : 1 : 1.53
	theor calcn	structure A	1.60 : 1 : 1.37
		structure B	1.30 : 1 : 0.60
		structure C	1.30 : 1 : 0.98

[a]Analytically determined results.

distributions as shown in Figure 2-2. Electron diffraction patterns of these particles revealed that both kinds of 4-ATP/Q-PbS particles had the same rock salt structure as that of bulk PbS.[65] The average diameter of the 4-ATP/Q-PbS particles prepared with $[Pb^{2+}]/[S^{2-}]$= 1.2 was 28 Å with the standard deviation of 5.0 Å and that with $[Pb^{2+}]/[S^{2-}]$= 1.6 was 27 Å with standard deviation of 4.1 Å. Reflecting these size distributions, both kinds of PbS microcrystals did not give such structured absorption spectra as those reported for Q-PbS.[21,56] However, since the magnitude of the above standard deviations is smaller than twice of the unit crystallographic distance between Pb and S atom of PbS particles, it may be said that the prepared Q-PbS particles had a good monodispersity in a chemical sense. Nevertheless, since Q-PbS particles intrinsically exhibit large quantum size effects,[15] appreciable variations in its band gap are anticipated for the size distributions as shown in Figure 2-2. However, the presence of Q-particles having different energy gaps does not bring about any serious problems in the present study, because relative comparisons of photoreduction behaviors of MV^{2+} at the two kinds of 4-ATP/Q-PbS particles having almost the same average size and very near size distribution are the main subject, as will be shown below.

The compositions of the two kinds of 4-ATP/Q-PbS particles are given in Table 2-1 in a relative ratio of Pb^{2+} : S^{2-} : $NH_2C_6H_4S^-$. It is seen that the particles prepared with

$[Pb^{2+}]/[S^{2-}]$= 1.6 contained larger fractions of Pb^{2+} and $NH_2C_6H_4S^-$ than those prepared with $[Pb^{2+}]/[S^{2-}]$= 1.2. Considering that the average size and size distribution of PbS microcrystals were not greatly different between the two kinds of PbS microcrystals as described above, the observed difference in the chemical composition seems to suggest that the surface structure of the two kinds of PbS microcrystals was very different, as already noted in chapter 1.

Using above experimental data of the size distributions, crystal structure and compositions of the 4-ATP/Q-PbS particles, I could evaluate the surface structures of both kinds of 4-ATP/Q-PbS particles. The procedures of identification of the surface structures of surface-modified Q-PbS particles were described in chapter 1. Theoretical compositions of the 4-ATP/Q-PbS particles predicted for three different surface structures which were postulated in as shown in Figure 1-6 are listed in Table 2-1. By comparison of these compositions with the experimentally determined ones, it is found that structure B, which has a partially covered surface with 4-ATP, is predominant in the surface of PbS particles prepared with $[Pb^{2+}]/[S^{2-}]$= 1.2, while structure A which gives a fully covered surface is predominant in the surface prepared with $[Pb^{2+}]/[S^{2-}]$= 1.6.

2-2-2 Surface Charge of PbS Microcrystals Modified with 4-ATP

FT-IR spectra of the two kinds of 4-ATP/Q-PbS particles showed that a -SH band observed 2550 cm^{-1} of 4-ATP molecules disappeared but not so for $-NH_2$ bands which appeared at 3440 and 3360 cm^{-1}. The result suggests that 4-ATP was bound to PbS microcrystals through sulfur atoms and that the amino groups of 4-ATP were present on the PbS surface. It is expected that the amino groups of the 4-ATP/Q-PbS particles have abilities for protonation, depending on the pH of solutions in which the PbS particles are suspended. To have information about this, potentiometric titration of the suspensions[105-107] was carried out. Figure 2-3(a) gives examples of titration curves. The amount of the surface charge (σ) against the unit mole of PbS was estimated from

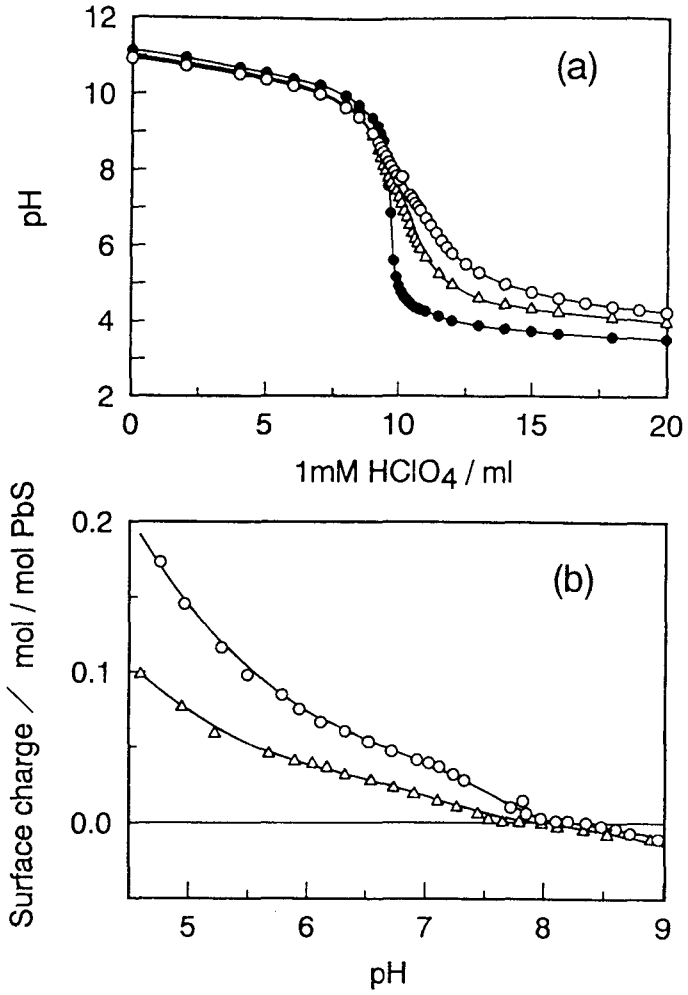

Figure 2-3 Potentiometric titration curves of 2.5 x 10^{-3} M 4-ATP/Q-PbS in 1.0 x 10^{-3} M NaOH solution with 1.0 x 10^{-3} M $HClO_4$ (a), and amount of surface charges of PbS particles calculated by eq. 2-1 (b). (○): the 4-ATP/Q-PbS particles prepared with $[Pb^{2+}]/[S^{2-}]$= 1.6. (△): that prepared with $[Pb^{2+}]/[S^{2-}]$= 1.2. (●): the titration curve obtained in the absence of suspended Q-PbS particles.

differences of pH in the solutions in presence and absence of the PbS particles by using the following equation.[106,107]

$$\sigma = - \frac{\{(C_H - C_{OH})_{PbS} - (C_H - C_{OH})_{int}\}}{[PbS]_0} \frac{(V_0 + \Delta V)}{V_0} \qquad (2\text{-}1)$$

where V_0 is the initial volume of the suspension, ΔV is the amount of the titrant used, $[PbS]_0$ is the molar concentration of the suspended PbS at V_0, $(C_H - C_{OH})_{PbS}$ and

$(C_H - C_{OH})_{int}$ are the difference in the concentration of protons and hydroxide ions in the presence and absence of the 4-ATP/Q-PbS particles, respectively. By application of this equation to the titration curves given in Figure 2-3(a), the surface charge as given in Figure 2-3(b) was obtained. At pHs lower than 8, both kinds of the 4-ATP/PbS particles have positive surface charges, which may result from protonation of either amino groups of the capped 4-ATP surface layer or sulfide ions of the unmodified PbS core surface or the both. Considering the experimental results that the amount of surface charges are greater at the PbS particles prepared with $[Pb^{2+}]/[S^{2-}]= 1.6$ which has a higher coverage with the capped 4-ATP than those prepared with $[Pb^{2+}]/[S^{2-}]= 1.2$, the positive charges must result mainly from the protonation of amino groups of the capped 4-ATP. However, if the ratio of the amount of surface charges of the 4-ATP/Q-PbS particles prepared with $[Pb^{2+}]/[S^{2-}]= 1.6$ to that prepared with $[Pb^{2+}]/[S^{2-}]= 1.2$ is obtained for various pHs lower than 8, it is found that the obtained ratio is a little smaller than that expected from the difference in the amount of the capped 4-ATP molecules between the two kinds of the 4-ATP/Q-PbS particles. Then I cannot rule out possibilities of the contribution of the protonation of sulfide ions of the unmodified PbS core surface to building up the positive charges of the 4-ATP/Q-PbS particles. Since the pKa of 4-ATP molecules is 4.3,[104] it is expected that the amount of protonated 4-ATP increases remarkably with decreasing pH from 6 to 3. However, as shown in Figure 2-3(b), a gentle increase in the amount of surface charges began to occur at pH 8. This finding seems to imply that the pKa of 4-ATP in the surface layer of the PbS microcrystals is different from that of 4-ATP molecules in solution, probably due to intramonolayer interactions. Similar discrepancies in protonation behaviors were observed at a self-assembled 4-ATP monolayer on gold electrodes.[104]

At pHs higher than 8, on the other hand, both kinds of the 4-ATP/Q-PbS particles have a very little negative surface charges. Since the amount of the negative surface charges seems to be a little greater at the PbS particles prepared with $[Pb^{2+}]/[S^{2-}]= 1.2$ which has a partially modified surface with 4-ATP, the negative surface charges may be

related to the sulfide ions present on the unmodified surface of the 4-ATP/Q-PbS particles. As shown in the figure, however, the amount of the negative surface charges of the 4-ATP/Q-PbS particles is very small compared to that of positive surface charges at pHs lower than 8, the surface of the 4-ATP/Q-PbS particles at pHs higher than 8 may be regarded to be electrically neutral.

2-2-3 Photoinduced Charge Transfer Reactions

PbS microcrystals of the diameter of about 30 Å or less have the potential of the conduction band negative enough to reduce methylviologen (MV^{2+}),[21,56] whose redox potential is -0.45 V vs. NHE.[71] The PbS particles prepared in the present study belonged to this class and then their photoreduction behaviors of MV^{2+} were investigated as a function of the surface charge of the PbS particles, as was previously done.[86,87,90,91,107] Irradiation with a 500 W Xe lamp of the 4-ATP/Q-PbS suspension containing MV^{2+} and sodium tartrate as a hole scavenger, resulted in the formation of methylviologen radical cations ($MV^{\bullet+}$) which were identified by characteristic absorption peaks at 396 nm and 606 nm.[72] The concentration of $MV^{\bullet+}$ was calculated based on the absorption peak at 396 nm, using the absorption coefficient of ε_{396}= 42100 $M^{-1}cm^{-1}$.[72] Judging from the finding that no absorption peak appeared at 540 nm,[108,109] the dimerization of $MV^{\bullet+}$ did not occur under my experimental conditions. During the course of Irradiation, the absorption spectra of the two kinds of 4-ATP/Q-PbS particles themselves were not changed at all, suggesting that they were not photocorroded. Figure 2-4 shows changes in absorbance at 396 nm caused by photoinduced formation of $MV^{\bullet+}$. A linear increase in the absorbance at 396 nm is seen for solutions having three different proton concentrations in an early stage of irradiation where the concentration of $MV^{\bullet+}$ is relatively low, but the rate of the absorbance increase slows down with an increase of the concentration of $MV^{\bullet+}$, suggesting that reoxidation of $MV^{\bullet+}$ by the photogenerated holes takes part in the photoinduced reactions.

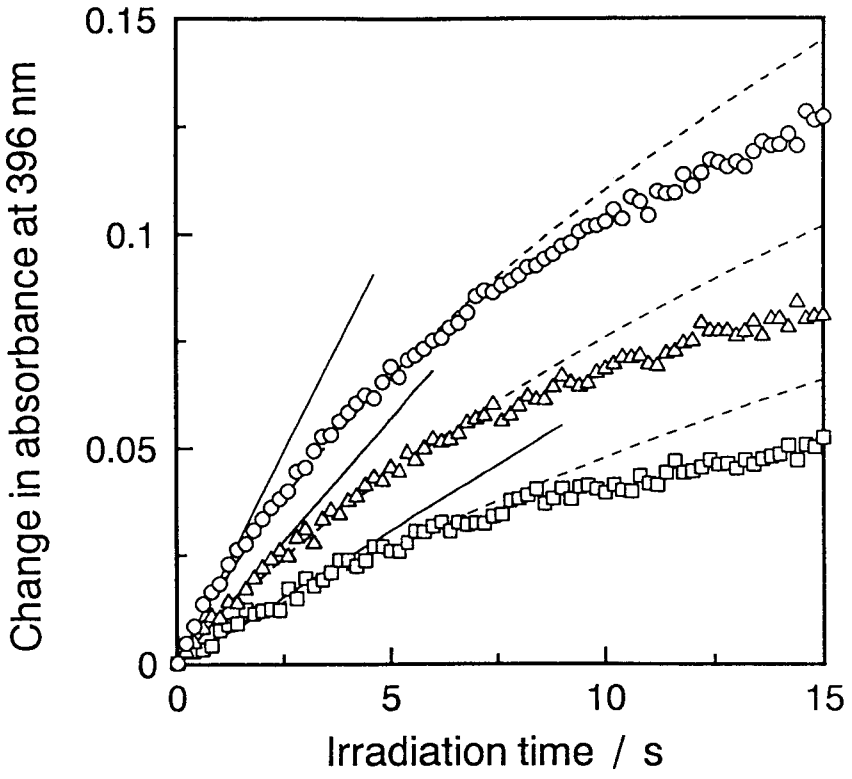

Figure 2-4 Changes in absorbance at 396 nm caused by photoreduction of MV^{2+}. 2.0 x 10^{-4} M 4-ATP/Q-PbS prepared with $[Pb^{2+}]/[S^{2-}]$= 1.6 were suspended in aqueous solutions containing 1.0 x 10^{-3} M MV^{2+} and 0.1 M sodium tartrate at pH 4.4 (○), 6.6 (△) and 9.0 (□). Straight lines show the gradient of absorbance change vs. irradiation time relations and dashed curves are calculated with eq. 2-9 using H values of 6.0 x 10^5 M^{-1} (pH 4.4), 5.5 x 10^5 M^{-1} (pH 6.6) and 5.0 x 10^5 M^{-1} (pH 9.0).

The initial formation rate (r_0) of $MV^{\bullet+}$ was evaluated from the linear relation between the $MV^{\bullet+}$ production and irradiation time, observed for low concentrations of $MV^{\bullet+}$. If the concentration of sodium tartrate used as a hole scavenger was fixed to 0.1 M, the r_0 value obtained at pH 5.0 was eventually constant even if the concentration of MV^{2+} was varied from 5.0 x 10^{-4} to 4.0 x 10^{-3} M. Then I attempt to analyze the photoreduction behaviors of MV^{2+} with stressing the importance of hole transfers from the PbS microcrystals to the hole scavenger. Analyses based on electron transfer controls have already been published for photoreduction of MV^{2+}.[110]

If it is assumed that at any instant of irradiation, only a couple of electron and hole is photogenerated in an irradiated microcrystal, then the rate of the deactivation with

recombination of them would be proportional to the number of photoexcited microcrystals.

$$PbS \xrightarrow{I_a} PbS^* \qquad : I_a \qquad (2\text{-}2)$$

$$PbS^* \xrightarrow{k_1} PbS \qquad : k_1[PbS^*] \qquad (2\text{-}3)$$

where I_a is the rate of photon absorption by each PbS microcrystal, and PbS^* represents a photoexcited PbS microcrystal in which a photogenerated e^--h^+ pair is contained, and k_1 is the rate constant for the deactivation with the recombination reaction. The right-hand side of the equations represents the rate of the respective reactions. Under the hole-transfer control, photogenerated electrons would get an opportunity to photoreduce MV^{2+} only when photogenerated holes are irreversibly transferred to hole scavengers.

$$PbS^* + Red_{ad} \xrightarrow{k_2} PbS(e) + Ox \qquad : k_2[PbS^*][Red_{ad}] \qquad (2\text{-}4)$$

$$PbS(e) + MV^{2+}{}_{ad} \xrightarrow{k_3} PbS + MV^{\bullet +} \qquad : k_3[PbS(e)][MV^{2+}{}_{ad}] \qquad (2\text{-}5)$$

$$PbS^* + MV^{\bullet +} \xrightarrow{k_4} PbS(e) + MV^{2+} \qquad : k_4[PbS^*][MV^{\bullet +}] \qquad (2\text{-}6)$$

where the subscript "ad" denotes adsorbed species on the 4-ATP/Q-PbS particles and PbS(e) represents a PbS microcrystal having one excited electron in it. By adopting steady state approximations for $[PbS^*]$ and [PbS(e)] in eq. 2-2 to 2-6, the rate of photoinduced formation of $MV^{\bullet +}$ is given by eq. 2-7.

$$\frac{d[MV^{\bullet +}]}{dt} = \frac{I_a k_2 [Red_{ad}]}{k_1 + k_2[Red_{ad}] + k_4[MV^{\bullet +}]} \qquad (2\text{-}7)$$

The rate constant k_3 of the electron transfer from the 4-ATP/PbS particles to MV^{2+}_{ad} (eq. 2-5) is not included in eq. 2-7, because I assume that the hole transfer reaction plays a key role in the all over reactions. If the concentration of $MV^{\bullet+}$ is very low, eq. 2-7 can be simplified to eq. 2-8.

$$\frac{d[MV^{\bullet+}]}{dt} = \frac{I_a k_2 [Red_{ad}]}{k_1 + k_2 [Red_{ad}]} = r_0 \qquad (2\text{-}8)$$

where r_0 denotes the initial formation rate of $MV^{\bullet+}$. Under the presence of a great of the hole scavengers in solution, $[Red_{ad}]$ can be regarded as to be constant due to adsorption equilibrium, and then I have a constant r_0 from eq. 2-8. This means that I can estimate r_0 by drawing straight lines in the $MV^{\bullet+}$ production vs. Irradiation time relations, as illustrated in Figure 2-4. Integration of eq. 2-7 gives eq. 2-9.

$$[MV^{\bullet+}] = \frac{1}{H} \{ -1 + (1 + 2H r_0 t)^{1/2} \} \qquad (2\text{-}9)$$

$$H = \frac{k_4}{k_1 + k_2 [Red_{ad}]} \qquad (2\text{-}10)$$

By inserting the determined r_0 into eq. 2-9 and by choosing best-fit values of H to meet the experimentally obtained absorption changes, dashed curves given in Figure 2-4 were obtained. Fairly good agreements are seen between experimental results and calculated ones in an early stage of the $MV^{\bullet+}$ production.

However, a little suppression in the production of MV^{2+} is seen in Figure 2-4 for a relatively long irradiation time. This must be caused by reoxidation of $MV^{\bullet+}$. One of the reoxidation process is given by eq. 2-6. In addition to this, another cause may be conceivable. As shown in Figure 2-2, relatively large particles with diameter around 40 Å

were a little contained in both kinds of 4-ATP/Q-PbS particles prepared in the present study. Such large particles did not have the abilities for photoreduction of MV^{2+},[21,56] so that $MV^{\bullet+}$ which was formed by reduction of MV^{2+} with the photogenerated electron transfer at small PbS particles would inject an electron to the conduction band of relatively large particles to regenerate MV^{2+}.

An equation similar to eq. 2-8 was derived by Mills and co-workers[111,112] with a different approach for photoreduction of MV^{2+} on bulk CdS particles. They assumed that the recombination rate of photogenerated charge carriers in n-type semiconductor particles is proportional to the concentration of the minority charge carriers (hole). As a result, there is a common feature between their model and mine in the point that photogenerated holes play an important role in the photoinduced reduction.

Figure 2-5(a) shows the effect of the concentration of tartrate as the hole scavenger on r_0, obtained in the presence of a high concentration of sodium chloride, 0.1 M. The high concentration of the electrolyte anions was used to keep the electrostatic interaction between the particle surfaces and MV^{2+} to be constant even in very dilute concentrations of sodium tartrate. As shown in the figure, the r_0 value increases with increasing the concentration of tartrate to 0.04 M, but beyond this concentration r_0 becomes almost constant. Saturated adsorption of tartrate anions must be achieved at this threshold concentration. In Figure 2-5(b), the best fit values of H given by eq. 2-9 to experimental results are shown, as a function of the tartrate concentration. Referring to eq. 2-10, it may be expected that the H values change with changes in the concentration of tartrate as well as r_0, but the obtained ones can be regarded to be almost the same for a wide concentration range of tartrate. This implies that a condition of eq. 2-11 holds under my experimental conditions.

$$k_1 >> k_2[Red_{ad}] \qquad (2\text{-}11)$$

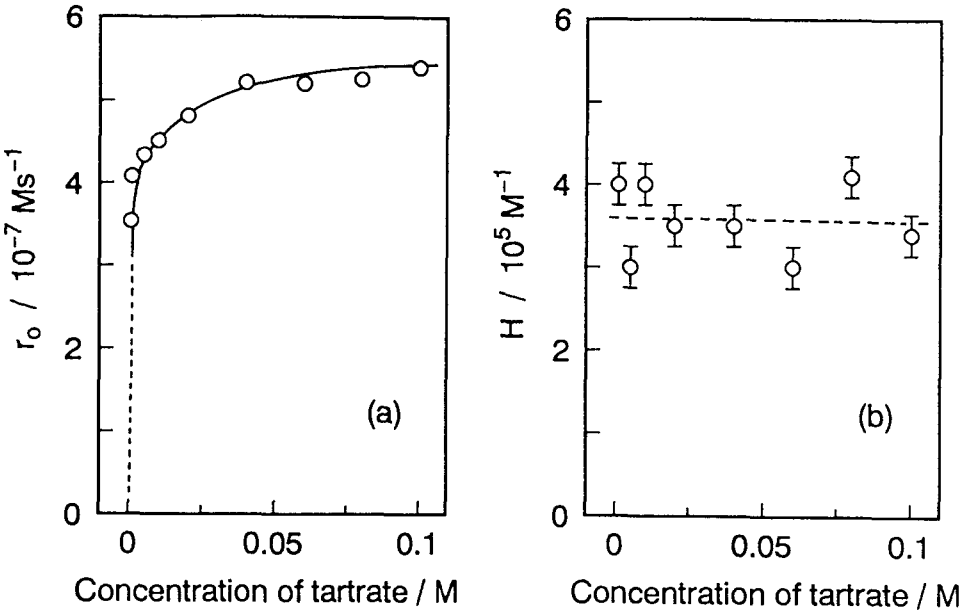

Figure 2-5 Effect of the concentration of sodium tartrate on the initial formation rate of $MV^{\bullet+}$ (a) and the best fit values of H given by eq. 2-9 to experimentally obtained absorbance changes (b). 2.0 x 10^{-4} M 4-ATP/Q-PbS was suspended in 0.1 M NaCl solutions at pH 5.0 containing 1.0 x 10^{-3} M MV^{2+} and a various concentration of sodium tartrate. The 4-ATP/ Q-PbS particles prepared with $[Pb^{2+}]/[S^{2-}]$= 1.6 was used.

The validity of eq. 2-11 was confirmed by determining the quantum efficiency for the $MV^{\bullet+}$ formation in an initial stage of irradiation. The quantum efficiency Φ_0 in that time period is given by r_0/I_a. Then rearrangement of eq. 2-8 gives eq. 2-12.

$$\frac{k_1}{k_2[Red_{ad}]} = \frac{1 - \Phi_0}{\Phi_0} \qquad (2\text{-}12)$$

The experimentally determined quantum efficiency for the $MV^{\bullet+}$ formation with Irradiation at 410 nm was about 0.6 % under experimental conditions of giving the highest r_0, and by applying this value to eq. 2-12, one can notice that eq. 2-11 is fulfilled.

As eq. 2-8 suggests, the initial rate would be influenced only by the concentration of the adsorbed hole scavenger $[Red_{ad}]$, which must be changed by the surface conditions like surface charges and surface structures of the 4-ATP/Q-PbS particles. Then the effects

of surface charges of the 4-ATP/Q-PbS particles on the photoinduced reaction of MV^{2+} were investigated using two kinds of hole scavengers of sodium tartrate and TEOA. In the case of using sodium tartrate, r_0 was found to increase remarkably with decreasing pH from pH 8, as shown in Figure 2-6(a). Especially notable for this was the 4-ATP/Q-PbS particles prepared with $[Pb^{2+}]/[S^{2-}]= 1.6$.

A principal cause for the observed increase in r_0 with a decrease in the pH is related to electrostatic interaction between the photocatalyst and tartrate anions. For pHs lower than 8, the 4-ATP/Q-PbS particles have positive charges as shown in Figure 2-3(b), while tartrate has negative charges (pKa 2.89, 4.16).[113] Then an attractive force must be operative between the surface of the 4-ATP/Q-PbS particles and tartrate anions, and its strength becomes enhanced with decreasing pH for a pH range investigated in this study, so that $[Red_{ad}]$ in eq. 2-8 is increased with decreasing pH. Since the positive surface charges are larger at the 4-ATP/Q-PbS particles prepared with $[Pb^{2+}]/[S^{2-}]= 1.6$, that is, $[Red_{ad}]$ is higher at the 4-ATP/Q-PbS particles prepared with $[Pb^{2+}]/[S^{2-}]= 1.6$ than that obtained at those prepared with $[Pb^{2+}]/[S^{2-}]= 1.2$, r_0 obtained is greater at the former photocatalyst than at the latter. It is expected that at pH 8, where the 4-ATP/Q-PbS particles have no net surface charges, no appreciable difference in r_0 appears between the two kinds of photocatalyst, but the results obtained are against this expectation. The difference in that case must result from the difference in the number of photons absorbed, as suggested from the results shown in Figure 2-1, though the genuine nature causing the absorbance difference is not known at present. By changing solution pH, the thermodynamic potential for oxidation of tartrate is changed. Then it might be speculated that such change is responsible for observed pH dependence of r_0. However, since the thermodynamic potential for oxidation of tartrate shifts negatively with an increase in the pH of solutions, it is expected to have an increase in r_0 with increasing the pH under the hole transfer control. The experimentally obtained results show a reverse tendency to such expectation.

When TEOA was used as a hole scavenger, pH dependencies of r_0 show opposite

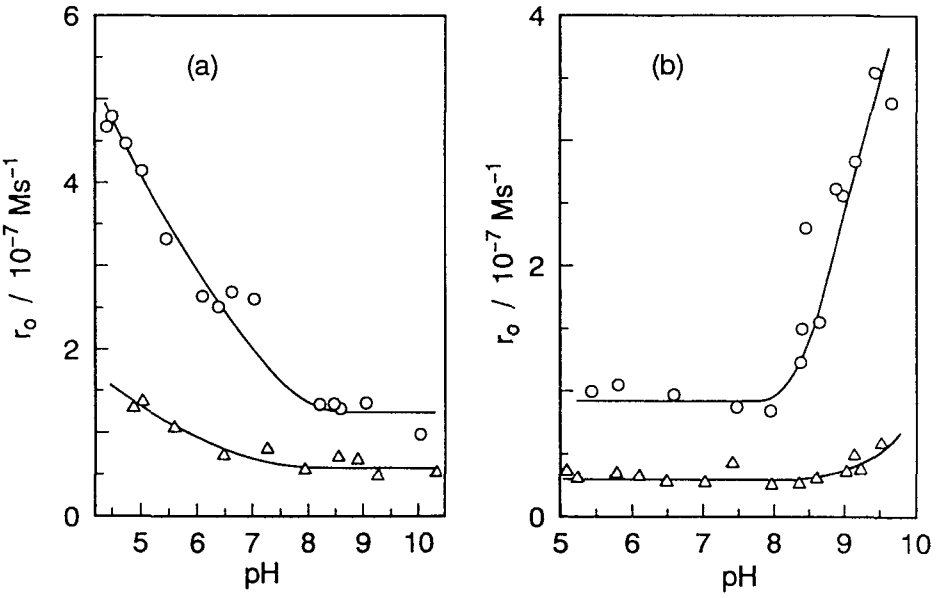

Figure 2-6 Effect of pH on the initial formation rate of $MV^{\bullet+}$ on the 4-ATP/Q-PbS particles in the presence of 0.1 M sodium tartrate (a) and 0.1 M TEOA (b) as the hole scavenger ([PbS]=2.0 x 10^{-4} M, [MV^{2+}]=1.0 x 10^{-3} M). The 4-ATP/Q-PbS particles prepared with [Pb^{2+}]/[S^{2-}]= 1.6 (○) and 1.2 (△).

tendencies to those obtained in the use of tartrate. With increasing the pH from 8, an increase in r_0 appeared as shown in Figure 2-6(b). It might be thought again that a negative shift of the oxidation potential of TEOA with an increase in pH is responsible for the appearance of the observed pH dependence of r_0. If this were the case, however, the same pH dependence of r_0 must appear between the two kinds of photocatalysts used, being in marked contrast to the experimental results. Then I have to find out another major cause responsible for the observed pH dependence on r_0.

As shown in the Figure 2-6(b), nearly constant r_0 values were obtained for pHs lower than 8 for both kinds of photocatalysts. In this pH region a repulsive force must be operative between the 4-ATP surface layer and protonated TEOA (pKa = 7.77).[113] Under such conditions a sufficient amount of adsorbed TEOA molecules is not available at photocatalyst surfaces, and a large fraction of photogenerated holes must be scavenged by TEOA molecules not adsorbed on but close to the 4-ATP/Q-PbS particles surfaces.

The rate of scavenging will be independent of pH in such cases, as observed. As in the case of using tartrate as a hole scavenger, r_0 was higher at the photocatalyst having the higher surface coverage with 4-ATP. One principal cause responsible for this may be due to the difference in the number of photons absorbed in two kinds of the photocatalysts. However, the magnitude of the difference in the r_0 in that case is a little greater than that expected from the difference in absorbed photons. One plausible explanation to account for this discrepancy is that although it is not rationalized from the point of the charged condition of the reactant and the 4-ATP/Q-PbS particles, a little amount of TEOA were adsorbed on the 4-ATP/Q-PbS particles with pH independency, the amount being higher at the photocatalyst having the higher coverage of 4-ATP.

For pHs higher than 8, a remarkable increase in r_0 is seen with increasing pH especially for the 4-ATP/Q-PbS particles prepared with $[Pb^{2+}]/[S^{2-}]= 1.6$, as shown in Figure 2-6(b). As shown in Figure 2-3(b), both kinds of the 4-ATP/Q-PbS particles have negative charges in this pH region, the amount being little larger at the 4-ATP/Q-PbS particles prepared with $[Pb^{2+}]/[S^{2-}]= 1.2$. If the negative charges were responsible for the observed increase in r_0, the effect therefore would appear more remarkably at this photocatalyst, being contradiction with the experimental results. Taking the pKa of TEOA into account, the amount of neutral TEOA becomes higher by increasing the pH from 8. If it is assumed that the neutral TEOA molecules can make adsorption on hydrophobic 4-ATP surface layers, then I can expect a higher reduction rate of MV^{2+} at the photocatalyst prepared with $[Pb^{2+}]/[S^{2-}]= 1.6$, as observed.

It is expected that inert electrolyte anions such as ClO_4^- may influence the rate of the MV^{2+} reduction at pHs lower than 8 if tartrate anions are used as the hole scavenger, because in such solution conditions the electrolyte anions and tartrate anions are competitively adsorbed on the positively charged 4-ATP/Q-PbS surfaces. In contrast, the inert electrolyte anions will have no remarkable influence on r_0 at pHs higher than 8 if TEOA is used as the hole scavenger. As shown in Figure 2-7, the initial formation rate of $MV^{\bullet+}$ obtained at pH 5.0 with use of tartrate as the hole scavenger was decreased by

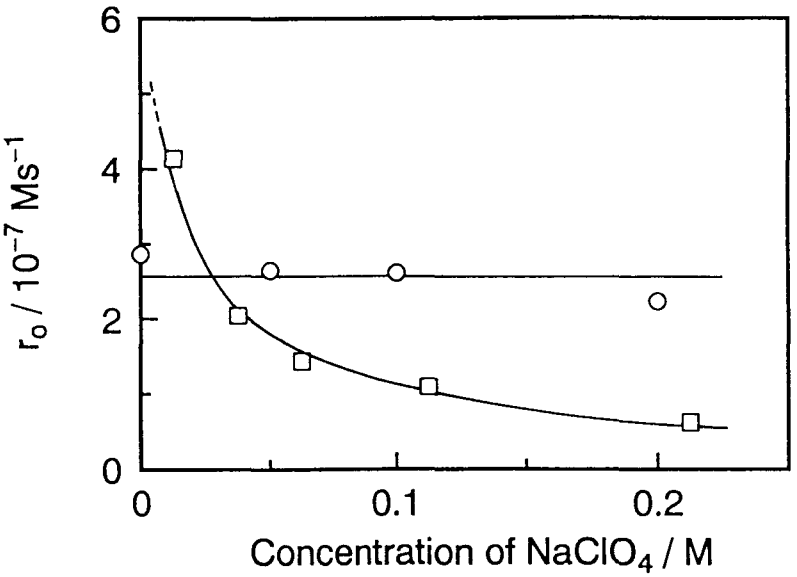

Figure 2-7 Effect of the concentration of ClO_4^- on the initial formation rate of $MV^{\bullet+}$ in 0.1 M sodium tartrate at pH 5.0 (□) and in 0.1 M TEOA at pH 9.5 (○). 2.0×10^{-4} M 4-ATP/Q-PbS prepared with $[Pb^{2+}]/[S^{2-}]= 1.6$ was used. $[MV^{2+}]=1.0 \times 10^{-3}$ M.

increasing the concentration of $NaClO_4$, as expected. In contrast, no effect of ClO_4^- and Na^+ ions was seen for the use of TEOA at pH 9.5, at which no repulsive or attractive interactions existed between the surface of photocatalyst and the hole scavenger. It should be noted that 0.1 M sodium tartrate solution at pH 5.0 contained ClO_4^- anions which were used to adjust the solution pH and whose amount was 1.26×10^{-2} M. Similarly 0.1 M TEOA solution at pH 9.5 contained 1.8×10^{-3} M ClO_4^-, even if no electrolyte was intentionally added.

2-3-4 Anion Effects on Photoinduced Charge Transfer

To obtain further insight into the effect of foreign electrolytes on the photoinduced reduction behavior of MV^{2+} in the presence of tartrate anions, I examined the effect of addition of NaCl, NaBr and $NaClO_4$ to 0.1 M sodium tartrate at pH 5.0 on the rate of photoreduction of MV^{2+}. According to the obtained results, which are given in Figure 2-8, the degree of the decrease of r_0 was very different among the kind of anions and was

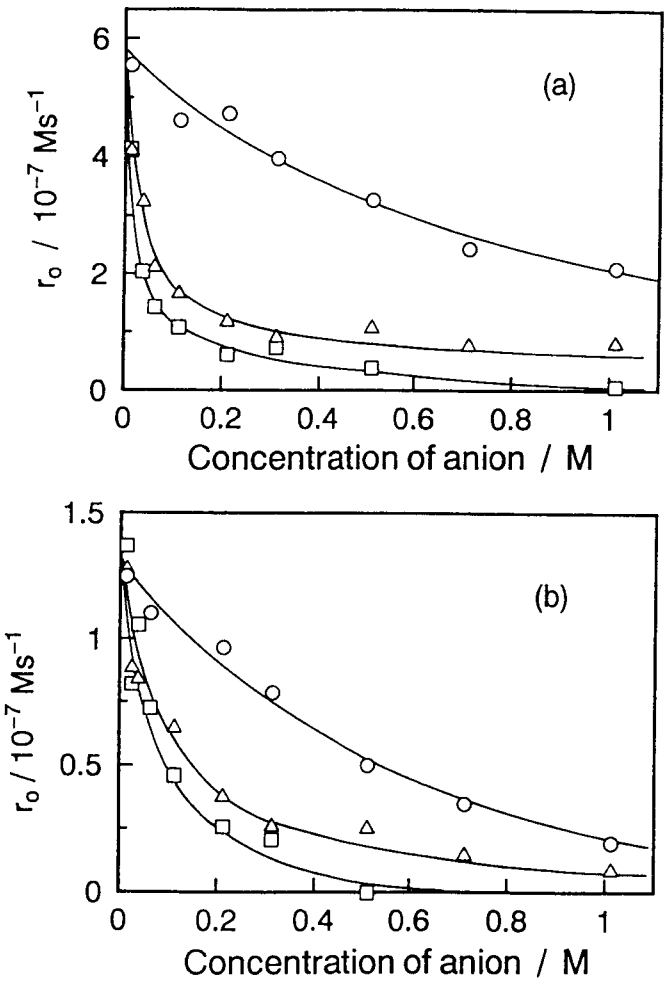

Figure 2-8 Effect of the concentration of Cl^- (○), Br^- (△) and ClO_4^- (□) on the initial formation rate of $MV^{\bullet+}$ using 0.1 M sodium tartrate at pH 5.0 for the 4-ATP/Q-PbS particles prepared with $[Pb^{2+}]/[S^{2-}]$= 1.6 (a) and 1.2 (b).

high in the following order, $ClO_4^- > Br^- > Cl^-$. These effects must be caused by different adsorbability of the anions onto the 4-ATP/Q-PbS particles.

To have a quantitative measure of the adsorption of tartrate anions and inert electrolyte anions on the 4-ATP/Q-PbS particles, the assumption is made that the adsorption occurs under the Langmuir adsorption equilibrium. At pH 5.0 tartrate anions mainly exist as dianions. For simplicity, I assume that only one carboxylate group of the dianion contributes to the adsorption. Even if the two carboxylate groups are involved in the adsorption of the dianion, the following discussion does not need any serious changes.

Only one necessary thing to do in that case is to read the fractional surface coverage of the tartrate anions given in eqs. 2-13 and 2-14 to be that of the dianions. The relation between the adsorption of tartrate anions T^- and the inert electrolyte anions X^- is represented by eq. 2-13.

$$K_T[T^-] / K_X[X^-] = \theta_T / \theta_X \qquad (2\text{–}13)$$

where θ_T and θ_X are the fractional surface coverage of T^- and X^-, respectively, and K_T and K_X are the adsorption equilibrium constant of T^- and X^-, respectively. The concentration of the adsorbed hole scavenger given by $[Red_{ad}]$ in eq. 2-8 should be proportional to θ_T as

$$[Red_{ad}] = S\,\theta_T \qquad (2\text{–}14)$$

where S is the maximum concentration of the adsorbed hole scavenger. Since the experimental results given by Figure 2-8 were obtained with the use of a relatively high concentration of sodium tartrate of 0.1 M, it may be assumed that tartrate anions adsorbed on the surface of the 4-ATP/Q-PbS particles make the saturated adsorption unless any other anions are available for adsorption. Then the assumption of $\theta_T + \theta_X = 1$ may be valid. Rearrangements of eq. 2-8 with use of eqs. 2-11, 2-13 and 2-14 with this assumption yield eq. 2-15.

$$\frac{1}{r_o} = \frac{k_1}{k_2 I_a S} \frac{K_X [X^-]}{K_T [T^-]} + \frac{k_1}{k_2 I_a S} \qquad (2\text{-}15)$$

By obtaining $1/r_o$ from the results shown in Figure 2-8 and by plotting it against the concentration of anions, I have linear relations between them, as shown in Figure 2-9. By applying eq. 2-15 to the results given in this figure, K_X/K_T is obtained, which is given in

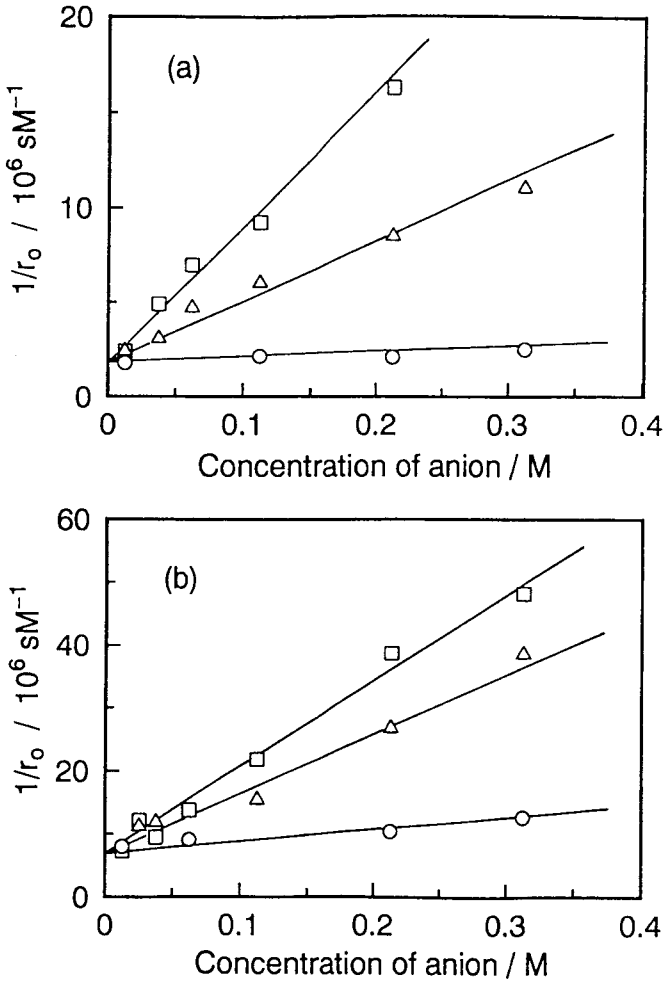

Figure 2-9 Relation between the reciprocal of the initial formation rate of $MV^{\bullet+}$ and the concentration of Cl^- (○), Br^- (△) and ClO_4^- (□) using 0.1 M sodium tartrate at pH 5.0 for the 4-ATP/Q-PbS particles prepared with $[Pb^{2+}]/[S^{2-}]$= 1.6 (a) and 1.2 (b).

Table 2-2. The K_X/K_T value increases in the order of $Cl^- < Br^- < ClO_4^-$, indicating that ClO_4^- has the highest adsorbability on the 4-ATP/Q-PbS particles. It was reported for self-assembled monolayer films of ω-hydroxythiol on gold that anions which have a higher hydration enthalpy are more easily penetrated into the modified hydrocarbon layer.[95] The results obtained here are in qualitative agreements with that view, since the hydration enthalpy (ΔH) of anions increases in the order of $Cl^- < Br^- < ClO_4^-$.[114] The anions having the higher hydration enthalpy must be more easily adsorbed on the hydrophobic organic layer of 4-ATP on the PbS particles.

Table 2-2 Ratio of K_X/K_T at Various Anions

$[Pb^{2+}]/[S^{2-}]$	surface structure	anion	K_X/K_T
1.2	structure B (partially modified PbS)	ClO_4^-	2.28
		Br^-	1.34
		Cl^-	0.181
1.6	structure A (fully modified PbS)	ClO_4^-	3.10
		Br^-	1.16
		Cl^-	0.140

Another interesting finding given in Table 2-2 is that the difference in the magnitude of K_X/K_T observed among the kind of electrolyte anions is larger for the 4-ATP/Q-PbS particles prepared with $[Pb^{2+}]/[S^{2-}]$= 1.6 rather than for those prepared with $[Pb^{2+}]/[S^{2-}]$= 1.2. In other words, the latter particles showed less selectivity for electrolyte anions. This finding is explained well on the basis of the difference in the surface structure of PbS particles. The 4-ATP/Q-PbS particles prepared with $[Pb^{2+}]/[S^{2-}]$= 1.2 has a partial coverage by 4-ATP, giving a less hydrophobic organic layer and consequently a less selectivity for the kind of electrolyte anions.

2-3 Conclusion

I prepared the two kinds of PbS microcrystals modified with 4-aminothiophenol, which had different amounts of positive surface charges in solutions of the pHs lower than 8. The photoinduced reduction of MV^{2+} using these PbS particles were influenced by both the pH of the solution and the kind of hole scavengers. In the case of sodium tartrate used as a hole scavenger, the photoinduced reduction of MV^{2+} was hindered by the inert electrolyte anions such as ClO_4^-. The results are explained well in terms of competitive adsorption of tartrate anions and inert anions on the surface of PbS particles. The effect of the inert anions was found to be influenced by the hydration enthalpy of the anions and furthermore by the surface structure of the PbS particles.

Chapter 3

Photoelectrochemical Properties of Size-Quantized CdS Microcrystals Modified with Various Amounts of Viologen-Functionalized Thiol

3-1 Introduction

One of potential applications of Q-particles would be the use as photocatalysts, where effective use of photogenerated electrons in Q-particles is essential to construct efficient light energy conversion systems. To achieve this, electron transfers from Q-particles to acceptors in solution have been investigated fairly intensively.[1,2,6-9] Since a high concentration of the acceptors on Q-particles surface is desired for the electron transfer to take place efficiently, various approaches have been tested such as the use of electrostatic interaction between Q-particle surface and acceptors,[77,84-88] the immobilization of acceptors in cyclodextrin as the host molecule bound to Q-particle surface[115] and the incorporation of Q-particles into polymer matrices having redox properties. The utility of the last approach has been demonstrated for Q-TiO_2[116,117] and Q-CdS[118] using viologen polymers where photogenerated electrons in the Q-particles transferred to the viologen groups of polymers.

One of interesting topics in the researches on the surface-modified Q-particles will be to attach new functionalities to the Q-particles,[35,92,93] such as pH sensitive photocatalytic activities with use of amino group of the thiol compound as demonstrated in the former chapter, but no study has been reported on photoinduced charge transfers from Q-particles to surface-bound redox groups. In this section the preparation of Q-CdS particles chemically modified with a redox-active thiol having viologen group is described. Furthermore the photoreduction behaviors of surface-modified viologen group as a function of its amount will be clarified and the abilities for electron mediation of the bound viologen will be demonstrated.

3-2 Experimental Section

1-Decyl-1'-(3-mercapto)propyl-4,4'-bipyridinium dibromide (VSH) was synthesized according to literature procedures.[98,99] The synthesized compound was identified by ^1H NMR and IR spectra, and was recrystallized from ethanol under N_2 atmosphere prior to use. Sodium bis (2-ethylhexyl) sulfosucinate (AOT) of reagent grade obtained from Aldrich was used as received. Other chemicals used in this study were of reagent grade and purchased from Wako Pure Chemical Industry. Pyridine and DMSO were used after distillation.

Q-CdS having various amounts of the bound VSH was prepared using inverse micelles.[24,25] 7.0 g of AOT and 2.0 cm^3 of distilled water were added to 100 cm^3 heptane to prepare an inverse micelle solution. 0.24 cm^3 of 1.0 M $Cd(ClO_4)_2$ aqueous solution and 0.16 cm^3 of 1.0 M Na_2S aqueous solution were added to 60 cm^3 and 40 cm^3 of the inverse micelle solution, respectively. After stirring individually for 1 h, these two kinds of solutions were mixed and stirred for 1 h, resulting in the formation of Q-CdS in the inverse micelles.

For the modification of the Q-CdS with different amounts of VSH, methanol solutions containing different amounts of VSH and 1-decanethiol (RSH), whose total concentration was fixed to 0.10 M, were prepared. 1.0 cm^3 of the methanol solution was added to 100 cm^3 of this inverse micellar solution and stirred for one day to modify the surface of Q-CdS with both VSH and RSH, the degree of the surface modification with VSH being dependent on the molar fraction of VSH to the sum of VSH and RSH in the methanol solution used. By adding pyridine to the inverse micelles, the thiol-modified Q-CdS particles were isolated, and then dried under vacuum. These particles were successively washed with heptane, petroleum ether and methanol, followed by drying again under vacuum. These procedures were carried out under N_2 atmosphere. The obtained Q-CdS particles are denoted in this section as V(x)/Q-CdS, where x represents the molar fraction of VSH to the sum of VSH and RSH used for surface modification. Q-

CdS particles modified with RSH only are denoted as R/Q-CdS.

Transmission electron microscopy (TEM) and electron diffraction analyses were performed with a Hitachi H-9000 transmission electron microscope at operation voltage of 300 kV. The samples for TEM were prepared by dropping Q-CdS dissolved in pyridine onto amorphous carbon overlayers on a Cu grid. To determine the composition of V(x)/ Q-CdS and R/Q-CdS, weight fractions of C, H, and N of particles were determined by elemental analyses and that of Cd by atomic absorption spectroscopy. Elemental analyses and atomic absorption spectroscopy were performed using a Yanaco Model MT-2 analyzer and a NJA AA-8500 Mark II spectrophotometer, respectively.

To investigate the photoinduced charge transfer from Q-CdS to the surface-bound viologen groups, 2.1 x 10^{-4} M Q-CdS was dissolved in a mixed solution of DMSO and pyridine (2 : 1) containing 1.0 x 10^{-3} M triethanolamine as a hole scavenger. 3.0 cm^3 of this solution was put in a quartz cell (1 cm x 1 cm x 4 cm height), evacuated to remove dissolved O_2, and finally filled with N_2. Then the solution was irradiated with a 500 W Xe lamp through a UV-cut off filter ($\lambda > 400$ nm). Absorbance changes of the solution caused by the irradiation were measured with use of a Hewlett Packard 8452A diode array spectrophotometer. The quantum efficiency of the reduction of the surface-bound viologen groups was determined based on the initial formation rate of viologen radical cations with irradiation at 400 nm. The photon flux was measured using a thermopile, Eppley lab. Model E-6. When the electron mediation of the surface-bound viologen groups was investigated, 2.0 x 10^{-5} M methylene blue (MB^+) or eosin-Y (EO-Y) was added to the above solution as an electron acceptor. Irradiation in that case was made using light of wavelengths covering from 400 to 450 nm to avoid photoexcitation of MB^+ and EO-Y. Changes in the concentration of MB^+ and EO-Y were determined by measuring absorbance at 670 and 540 nm with the absorption coefficients of 9.5 x 10^4 [119] and 9.7 x 10^4 M cm^{-1},[120] respectively.

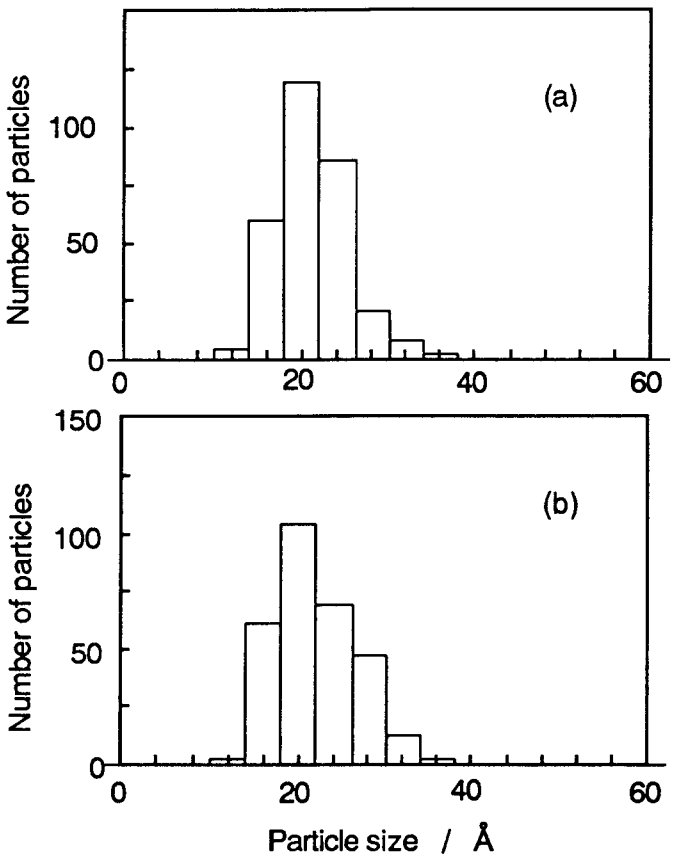

Figure 3-1 Size distribution of V(1.0)/Q-CdS (a) and R/Q-CdS (b).

3-3 Results and Discussion

3-3-1 Characterization of CdS Microcrystals Modified with Viologen-Functionalized Thiol

The Q-CdS particles prepared with various fractions of VSH gave almost the same absorption spectra ; the absorption peak due to excitonic transition appeared at 400 nm and absorption threshold was 480 nm, suggesting that V(x)/Q-CdS particles had the same particle size distributions independent of x values. This suggestion was confirmed by TEM observations. Their size distributions obtained from TEM images are shown in Figure 3-1 for the V(1.0)/Q-CdS and R/Q-CdS. The average size of the former particles was 21 Å with the standard deviation of 3.9 Å and that of the latter particles was 22 Å with

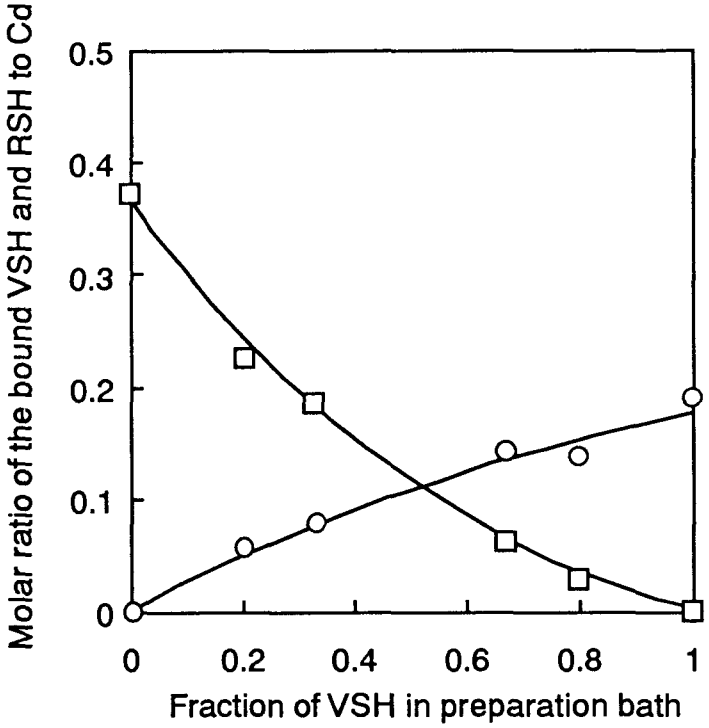

Figure 3-2 The amount of the bound VSH (○) and RSH (□) as a function of the mole fraction of VSH to the sum of VSH and RSH used in the surface modification of Q-CdS.

the standard deviation of 4.4 Å. In all cases Q-CdS particles prepared were spherical and had a cubic structure.

IR spectra of V(1.0)/Q-CdS and R/Q-CdS showed that absorption due to -SH vibration at 2600 cm^{-1} which was observed for VSH and RSH molecules was absent, resulting that these molecules bound to Q-CdS through S atoms. The amount of VSH and RSH bound to the Q-CdS was calculated based on the experimentally determined weight fraction of C, H, N and Cd, as follows. The molar ratio of C, H and N obtained for V(1.0)/ Q-CdS was in agreement with that expected from the chemical formula of VSH-derived thiolate, and the same was true for R/Q-CdS. Other V(x)/Q-CdS had different weight fraction of C, H, and N from that obtained for V(1.0)/Q-CdS and R/Q-CdS, as expected from chemical modification with both VSH and RSH. Since a VSH molecule contains two nitrogen atoms but an RSH molecule dose not, the amount of the bound VSH of V(x)/ Q-CdS was straightforwardly determined from elemental analyses results of nitrogen.

Then by subtracting the theoretically predicted amount of carbon of the bound VSH from analytically determined total carbons, the amount of the bound RSH was evaluated. The molar ratios of the surface bound RSH and VSH to the total Cd of Q-CdS, which are represented in this paper as f_V and f_R , respectively, were then obtained referring to the amount of Cd determined for V(x)/Q-CdS. Figure 3-2 shows f_R and f_V as a function of the molar fraction of VSH to the total thiol molecules (VSH and RSH) used in the surface modification of Q-CdS particles. With increasing the mole fraction of VSH in the surface modification procedure, f_V systematically increased , while f_R decreased. Since the size distribution of V(x)/Q-CdS was almost the same for different x values, the difference of the results given in Figure 3-2 show how the number of VSH and RSH bound to one CdS particle was influenced by the fraction of VSH used in the surface modification procedure. Referring to this figure, it is in principle possible to prepare any ratio of the surface-bound VSH to RSH by changing the relative mole ratio of VSH to RSH in the preparation bath.

Based on the results given in Figure 3-2, the coverage ratio of Q-CdS surface with the surface modifiers was evaluated. For this purpose the size distribution evaluated from the average of those of V(1.0)/Q-CdS and R/Q-CdS shown in Figure 3-1 was used to obtain the average volume of V(x)/Q-CdS. The result gave 5900 $Å^3$ as the average volume of a Q-CdS particle and 1600 $Å^2$ as the surface area. The number of CdS units included in the estimated volume, N^{av}_{CdS}, is then obtained to be 120, using the density of cubic CdS of 4.87 g cm^{-3}.[121] The degree of the surface coverage with the modifiers, Γ, is given by eq. 3-1.

$$\Gamma = \frac{(f_V S_V + f_R S_R) N^{av}_{CdS}}{S^{av}_{CdS}} \qquad (3\text{-}1)$$

where S_V and S_R are the area occupied by a bound VSH and RSH molecule on the Q-CdS

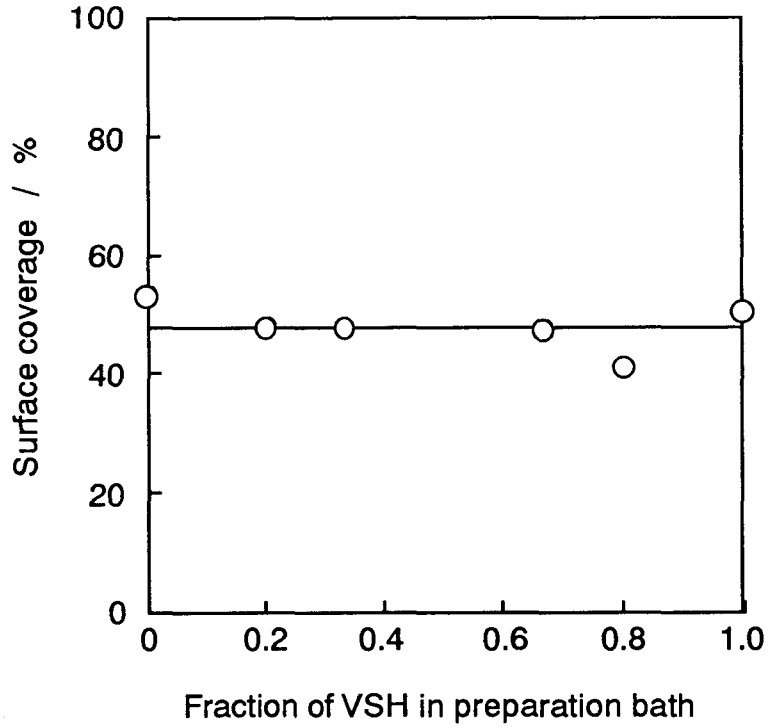

Figure 3-3 Degree of the surface coverage with thiols (VSH and RSH) of Q-CdS prepared with different fractions of VSH in the surface modification procedure.

surface, respectively, and S^{av}_{CdS} is the surface area of V(x)/Q-CdS of the average volume, 1600 Å^2. Calculations show that S_V and S_R are 35 and 19 Å^2 with use of the radii of the cross section of 3.35 and 2.43 Å for alkyl chain and bipyridyl ring, respectively.[122] By applying those values to eq. 3-1, Γ was evaluated for a variety of x, as shown in Figure 3-3. According to the results obtained, the degree of surface coverage with the surface modifiers was about 50 %, regardless of the molar fraction of VSH in the preparation bath. Judging from this finding, the bound VSH and RSH seemed to make a monolayer on the Q-CdS surface.

3-3-2 Photoinduced Charge Transfer from CdS Microcrystals to Surface-Bound Viologen

Continuous irradiation of V(x)/Q-CdS particles in the mixed solution of DMSO and pyridine (2 : 1) resulted in changes in absorption spectra, as shown in Figure 3-4(a), for

example, for the case of V(1.0)/Q-CdS. Absorption due to radical cations of the surface-bound viologen groups increased with an increase of the irradiation time. The absorption peak observed at around 538 nm is due to dimeric radical cations and that at around 606 nm monomeric ones.[108,109] The concentration of the viologen radical cation monomer (C_{mono}) and dimer (C_{dim}) was evaluated using eqs. 3-2 and 3-3.[109]

$$C_{mono} = \frac{\varepsilon_d^{538} A^{606} - \varepsilon_d^{606} A^{538}}{\varepsilon_m^{606} \varepsilon_d^{538} - \varepsilon_m^{538} \varepsilon_d^{606}} \qquad (3\text{-}2)$$

$$C_{dim} = \frac{\varepsilon_m^{606} A^{538} - \varepsilon_m^{538} A^{606}}{\varepsilon_m^{606} \varepsilon_d^{538} - \varepsilon_m^{538} \varepsilon_d^{606}} \qquad (3\text{-}3)$$

where ε_d^{538} and ε_d^{606} are the absorption coefficients of the viologen radical cation dimer at 538 and 606 nm, which are 23300 and 2600 M^{-1} cm^{-1}, respectively,[109] ε_m^{538} and ε_m^{606} are those of viologen radical cation monomer and are 5050 and 12200 M^{-1} cm^{-1}, respectively,[109] and A^{538} and A^{606} are absorbance at 538 and 606 nm, respectively. At any time of irradiation, the total concentration of viologen radical cations, C_{total}, is given by eq. 3-4

$$C_{total} = C_{mono} + 2\,C_{dim} \qquad (3\text{-}4)$$

The concentration of viologen radical cations evaluated in this way increased with an increase of the irradiation time, as shown in Figure 3-4(b) for V(1.0)/Q-CdS, but the increasing behaviors were a little different between the monomeric radical cations and the dimeric ones. At an early stage of irradiation shorter than 100 s, the formation of the latter was predominant, but beyond that time, its formation was declined, while the monomeric

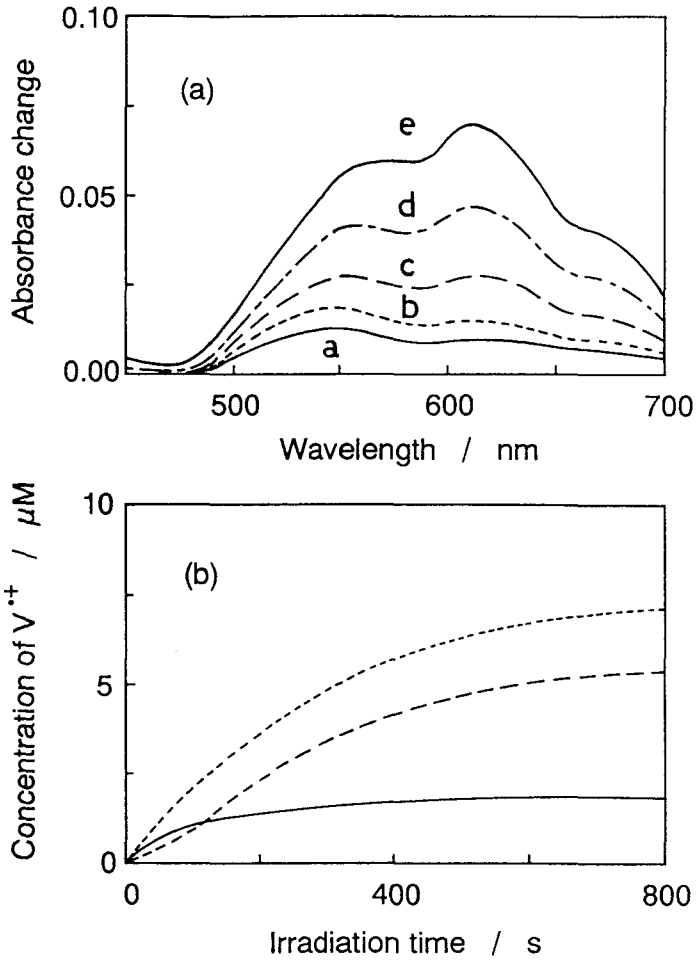

Figure 3-4 Changes in absorption spectra (a) and the concentration of monomeric viologen radical cations (- - -) and dimeric ones (———) (b), caused by irradiation with light of wavelengths longer than 400 nm of 2.1 x 10^{-4} M V(1.0)/Q-CdS in DMSO-pyridine (2 : 1) mixed solution containing 1.0 x 10^{-3} M triethanolamine. a; 20 s, b; 40 s, c, 80 s, d; 160 s, e, 320 s. The total concentration of viologen radical cations (- - - -) was calculated as the sum of the amount of monomeric radicals and dimeric ones. Irradiation intensity was 5.3 x 10^{-2} W cm^{-2}.

radical cations were produced at significant rates. The easiness of the dimer radical cation formation observed here are in quantitative agreement with the results reported for electrochemical reduction of a dimer-viologen molecule (1, 3-bis (N-ethyl-4, 4'-bipyridinium) propane).[109]

The sum of the steady-state concentrations of photo-formed monomeric and dimeric viologen radical cations became large with increase in f_V, as shown in Figure

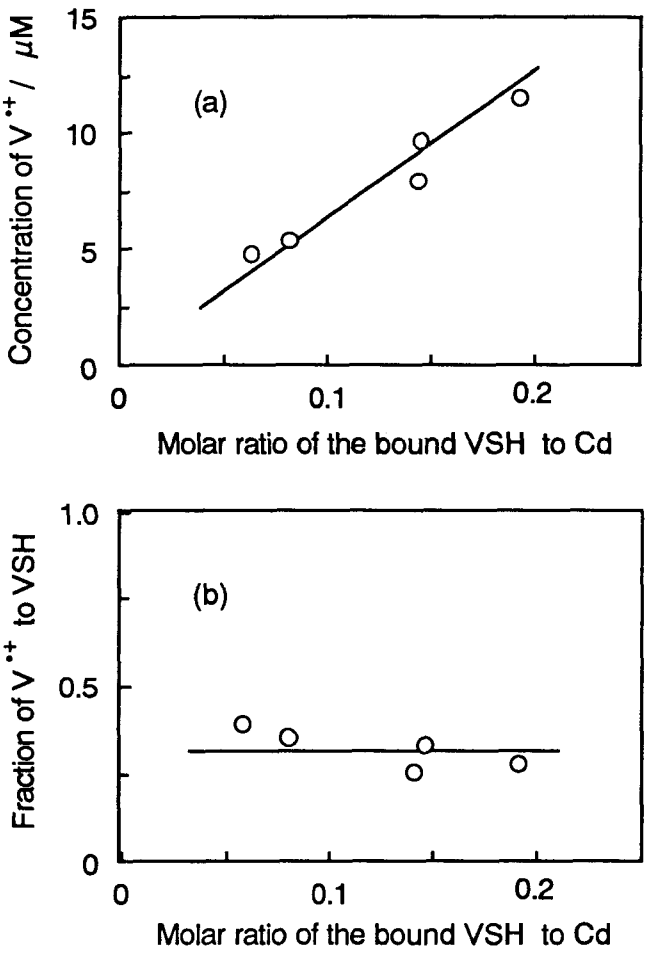

Figure 3-5 The sum of the steady state concentration of monomeric and dimeric viologen radical cations (a) and its fraction to the concentration of the bound VSH (b) for Q-CdS having different amounts of the bound VSH.

3-5(a). However, if this value is divided by the total concentration of the surface-bound viologen group that is obtained from the product of f_V and the concentration of CdS (2.1 x 10^{-4} M), a constant value was obtained, as shown in Figure 3-5(b). Since the potential of the conduction band of CdS is negative enough to reduce the viologens,[6] almost all the bound viologens should be reduced, but the experimental results obtained here show that this was not the case; as small as ca. 30 % of the surface-bound viologen groups were reduced. It seems reasonable to assume that reoxidation of the photo-formed radical cations by the valence band holes of Q-CdS occurred in competition with reduction of the surface-bound viologens by the conduction band electrons, giving in a constant fraction

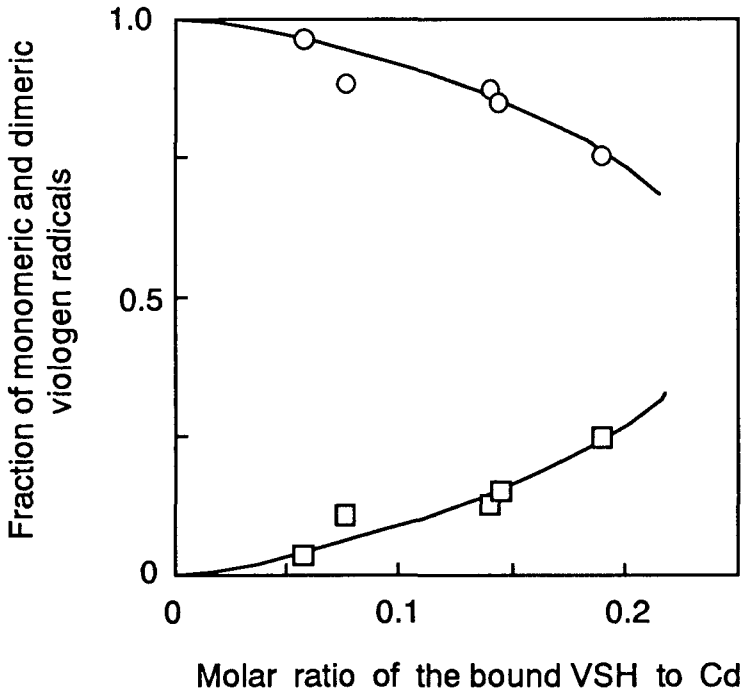

Figure 3-6 Dependence of the fraction of the steady state amount of monomeric (○) and dimeric (□)viologen radical cations on the amount of surface-bound VSH.

of radical cations under steady state conditions.

As already shown in Figure 3-5(b), the ratio of the sum of the photo-formed radical cations to the total amount of the bound viologen groups was independent of the amount of surface-modified VSH, but if the fraction of the concentration of the dimeric radical cations to that of the total reduced viologens is obtained, results shown in Figure 3-6 are obtained. In this figure, results obtained for the monomeric radical cations are also included. The dimeric radical cations increased with an increase in f_V , while a reverse tendency appeared for the monomeric one. These findings must reflect the situation that the surface-bound VSH became close to each other with an increase in f_V , favoring their association.

The photo-induced reduction of surface-bound viologen consists of a sequential charge transfers, as follows.

$$CdS \rightarrow e^- + h^+ \qquad (3\text{-}5)$$

$$e^- + h^+ \rightarrow h\nu, \Delta \qquad (3\text{-}6)$$

$$e^- + V^{2+} \rightarrow V^{\bullet+} \qquad (3\text{-}7)$$

$$2V^{\bullet+} \rightarrow (V^{\bullet+})_2 \qquad (3\text{-}8)$$

$$h^+ + V^{\bullet+} \rightarrow V^{2+} \qquad (3\text{-}9a)$$

$$h^+ + (V^{\bullet+})_2 \rightarrow V^{2+} + V^{\bullet+} \qquad (3\text{-}9b)$$

$$h^+ + Scav \rightarrow Scav^+ \qquad (3\text{-}10)$$

V^{2+}, $V^{\bullet+}$ and $(V^{\bullet+})_2$ in the above equations are a non-reduced viologen, its radical cation monomer and dimer, respectively, and Scav and $Scav^+$ are a hole scavenger and its oxidized form in solution, respectively. Since the potential of the valence band edge[6] is positive enough to oxidize $V^{\bullet+}$ and $(V^{\bullet+})_2$, and the difference of the redox potentials between the radical cation monomer and the dimer[109] is as small as 0.06 V, it may be assumed from the view point of the thermodynamics that the reaction rates of eqs. 3-9a and 3-9b are almost the same. Then in the derivation of the rate equation, eq. 3-9b may be included in eq. 3-9a with the use of C_{total} given by eq. 3-4 as the concentration of reduced viologen in the rate equations. In the present study, since the photoreduction of the surface-bound viologens was investigated under such low irradiation intensity that only one electron-hole pair and not two is produced simultaneously in a particle, the electron-hole recombination would follow a first order rate law.[123] If steady state approximations are adopted for the concentration of electron and holes under such irradiation conditions, then eq. 3-11 is derived.

$$d[e^-]/dt = d[h^+]/dt = I_a - k_r[pair] - k_f[e^-][V^{2+}] = 0 \qquad (3\text{-}11)$$

where I_a is the rate of photon absorption by Q-CdS and [pair] represents the concentration of photogenerated electron-hole pairs, k_r is the rate constant for the recombination, and k_f is that for electron transfers to the surface-bound viologen.

Since the formation of viologen radical cations competes with their reoxidation, the net rate of the radical cation formation is given by eq. 3-12,

$$d[V^{\bullet+}] / dt = k_f [e^-] [V^{2+}] - k_b [h^+] [V^{\bullet+}] \qquad (3\text{-}12)$$

where k_b is the rate constant for oxidation of radical cations by the valence band holes. Under steady state conditions, $[e^-]$ may be regarded to be equal to $[h^+]$, and then it is equal to [pair]. Rearrangements of eq. 3-11 give eq. 3-13.

$$[e^-] = I_a / (k_r + k_f [V^{2+}]) \qquad (3\text{-}13)$$

This equation predicts that the concentration of electrons in Q-CdS is changed by the concentration of non-reduced viologen bound on Q-CdS which is changed by irradiation time. The quantum efficiency for the initial formation of viologen radical cations (Φ_o) is represented by eq. 3-14 using eq. 3-13.

$$(1 - \Phi_o) / \Phi_o = k_r / (k_f [V^{2+}]_o) \qquad (3\text{-}14)$$

where $[V^{2+}]_o$ is the concentration of bound viologen groups. In cases where the quantum efficiency is low, a relation of $k_r >> k_f[V^{2+}]_o > k_f[V^{2+}]$ is obtained from eq. 3-14. Then eq. 3-13 is simplified to eq. 3-15.

$$[e^-] = I_a / k_r \qquad (3\text{-}15)$$

The experimentally obtained quantum efficiency for the initial formation of surface-

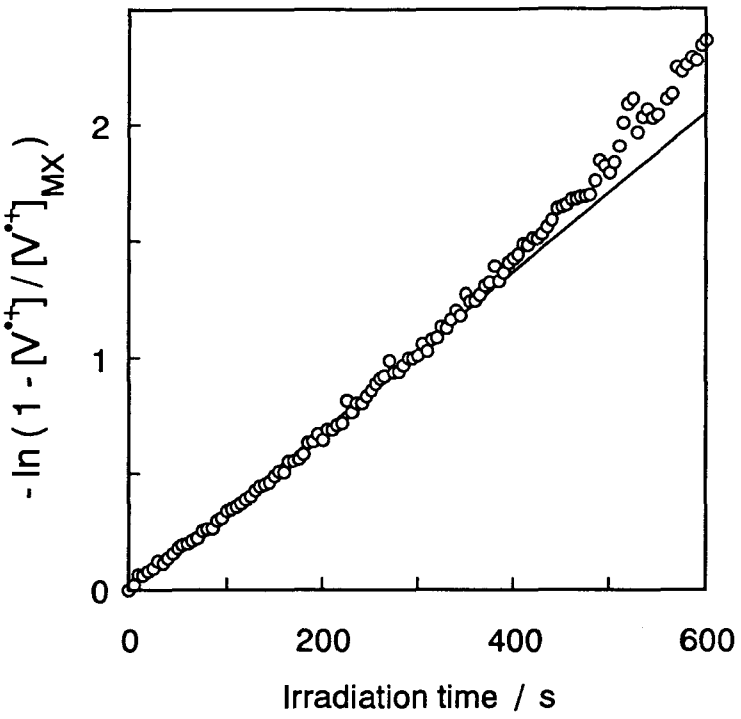

Figure 3-7 Plots of the left hand side of eq. 3-17 as a function of the irradiation time. The data used for the plots were obtained from results shown in Figure 3-4(b).

bound viologen radical cations was the highest at V(1.0)/Q-CdS, but the value obtained was as small as 2 %, This implies that $[e^-]$ is given by eq. 3-15 for all V(*x*)/Q-CdS. By integration of eq. 3-12 with use of eqs. 3-15 and 3-16,

$$k'_f = k_f I_a / k_r,\ k'_b = k_b I_a / k_r \qquad (3\text{-}16)$$

eq. 3-17 is obtained.

$$-\ln \{ 1 - [V^{\bullet+}] / [V^{\bullet+}]_{MX} \} = (k'_f + k'_b)\, t \qquad (3\text{-}17)$$

where $[V^{\bullet+}]_{MX}$ is the steady state concentration of photo-formed viologen radical cations and is given by eq. 3-18.

$$[V^{\bullet+}]_{MX} = \{ k'_f / (k'_f + k'_b) \} [V^{2+}]_o \qquad (3\text{-}18)$$

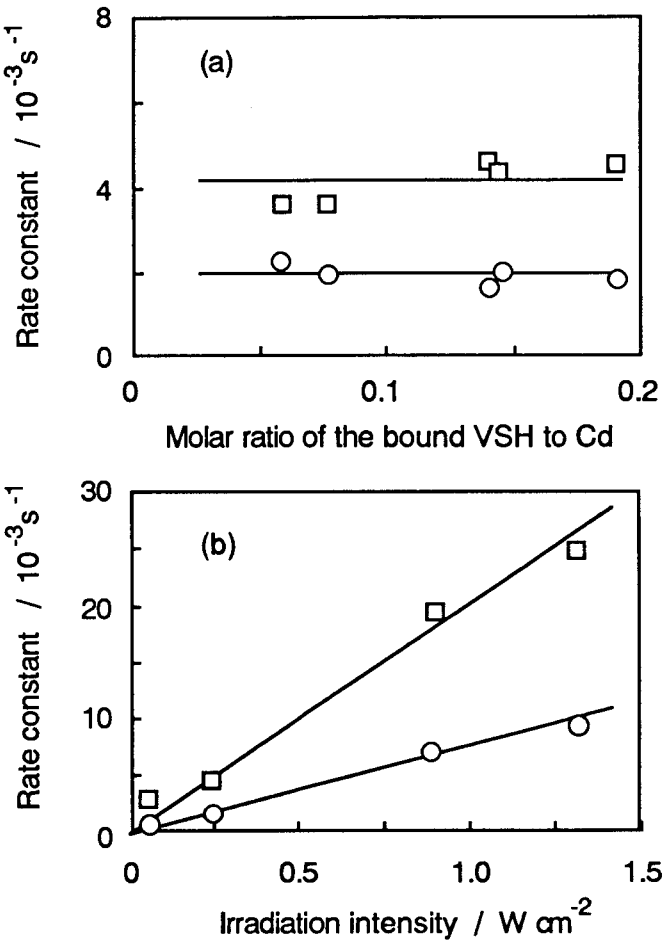

Figure 3-8 (a) Dependence of the rate constant for photoreduction of surface-bound VSH (k'_f) (○) and for reoxidation of the resulting viologen radical cations by valence band holes (k'_b) (□) on the amount of the bound VSH, obtained at constant irradiation intensity (2.4 x 10^{-1} W cm^{-2}). (b) Dependence of k'_f (○) and k'_b (□) on the irradiation intensity at V(1.0)/ Q-CdS.

The value of $[V^{\bullet+}]$ given in eq. 3-17 was obtained by applying eq. 3-4 to the results shown in Figure 3-4(b). As the value of $[V^{\bullet+}]_{MX}$, a saturated value of C_{total} was adopted. If the term of the left hand side of eq. 3-17 is obtained using $[V^{\bullet+}]$ and $[V^{\bullet+}]_{MX}$ obtained in this way, and is plotted as a function of the irradiation time for the case of V(1.0)/Q-CdS, Figure 3-7 is obtained. It is seen that a fairly good linear relation holds between them, and from the slope of the relation, $(k'_f + k'_b)$ is estimated. By inserting the obtained $(k'_f + k'_b)$ into eq. 3-18, k'_f and k'_b are determined.

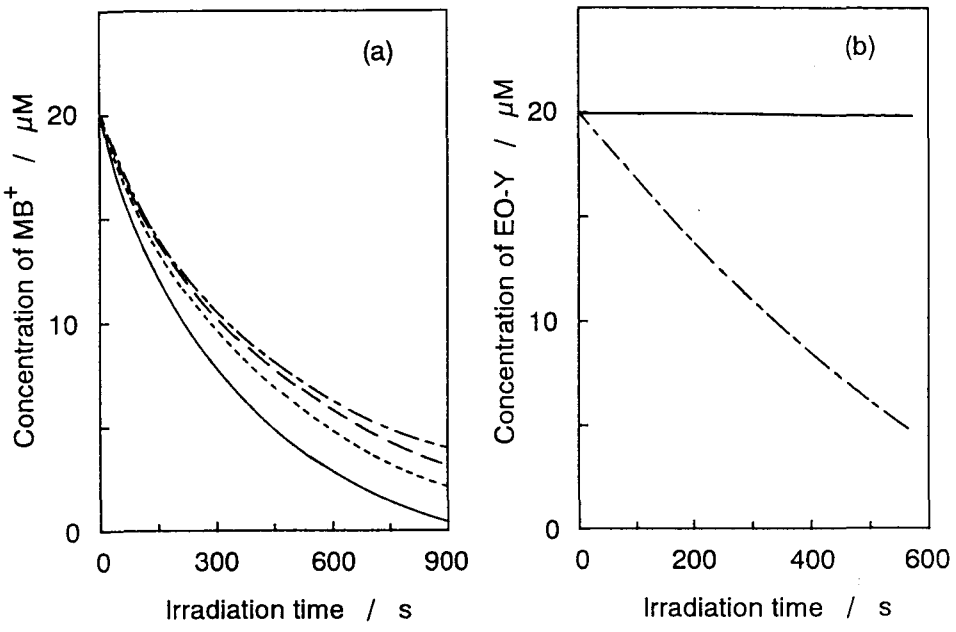

Figure 3-9 Changes in the concentration of MB^+ (a) and EO-Y (b) in DMSO-pyridine (2 : 1) mixed solution containing 2.1 x 10^{-4} M Q-CdS and 1.0 x 10^{-3} M triethanolamine. ——: V(1.0)/Q-CdS, - - - -: V(0.67)/Q-CdS, – – –: V(0.33)/Q-CdS, – - –: R/Q-CdS. Irradiation was performed with light of wavelengths covering 400 to 450 nm.

The k'_f and k'_b values obtained in this way for V(x)/Q-CdS particles are shown in Figure 3-8(a), which indicates that both k'_f and k'_b are invariant with the amount of the surface-bound viologen group. The results seem to suggest that the energy levels of Q-CdS is not changed by the amount of the surface-bound VSH, and the rate of its photoreduction is simply determined by the amount of the bound acceptor. The same is true for the reoxidation of the radical cations by the valence band holes; the rate of the reoxidation is determined by the amount of radical cations as long as the irradiation intensity is fixed. Furthermore the results shown in Figure 3-8(a) indicate that the reoxidation of photo-formed radical cations given by eqs. 3-9a and 3-9b occurred more rapidly than the forward electron transfer given by eq. 3-7. However if the irradiation intensity is changed, k'_f and k'_b are changed as a matter of course, as shown in Figure 3-8(b) for V(1.0)/Q-CdS, where it is shown that both k'_f and k'_b are proportional to the irradiation intensity, as predicted by eqs. 3-15 and 3-16.

3-3-3 Photoinduced Charge Transfer to Electron Acceptors in Solution

It is expected that surface-bound VSH has abilities of electron mediation for electron acceptors in solution if energetic correlations between them are feasible for such event to take place. To confirm the idea, photoreduction of MB^+ and EO-Y in solution were investigated using Q-CdS having different amounts of surface modified VSH. As shown in Figure 3-9(a), MB^+ was reduced at all Q-CdS particles used; x = 1.0, 0.67, and 0.33 for V(x)/Q-CdS and R/Q-CdS. Absorption peaks due to viologen radical cations did not appear for all cases until the reduction of MB^+ in solution was completed. Furthermore it was found that the rate of MB^+ reduction was larger for Q-CdS particles having the larger amount of the surface-bound viologen group. Since as shown in Figure 3-3, the surface coverage by the sum of VSH and RSH was almost the same for Q-CdS particles having different amounts of the bound VSH, the observed differences in the rate of reduction among the kind of Q-CdS particles must have resulted from the differences in the amount of the surface-bound viologen groups. In contrast to the photoreduction of MB^+, photoreduction of EO-Y took place at R/Q-CdS, but not at V(x)/Q-CdS, as shown in Figure 3-9(b). In cases of V(x)/Q-CdS, the surface-bound VSH was reduced in preference to reduction of EO-Y in solution. These results can be explained well in terms of the redox potentials of VSH, MB^+ and EO-Y in the mixed solution of DMSO-pyridine (2 : 1), which were determined to be -0.40, -0.26 and -1.29 V vs. SCE, respectively, with cyclic voltammetry. As shown in Figure 3-10, the photogenerated electrons in the conduction bands of Q-CdS are easily transferred to the surface-bound viologen to cause its reduction, and the reduced viologen quickly give electrons to MB^+ in solution. The process occurs more easily when the amount of surface-bound viologen is greater. The surface-bound viologens does not have any ability for reduction of EO-Y, and then EO-Y in solution is reduced with direct transfer of photogenerated electrons from Q-CdS, as illustrated in Figure 3-10(b). If the surface-bound VSH is available, photogenerated

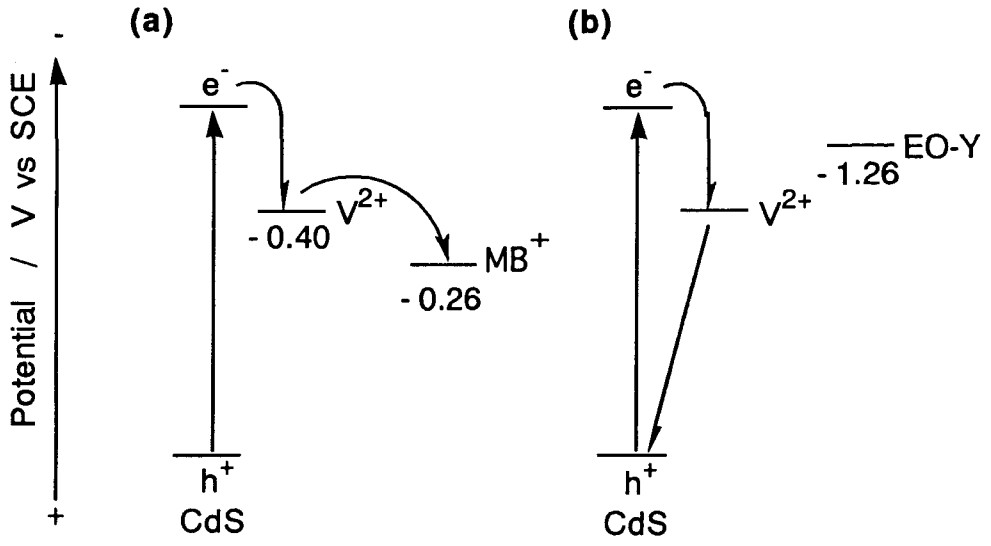

Figure 3-10 Energy diagram of the surface-bound viologen group, MB^+ (a) and EO-Y (b) in DMSO-pyridine (2 : 1) mixed solution.

electrons are more easily transferred to the VSH to cause its reduction. Since reoxidation of viologen radical cation becomes serious with increase in its amount, the reduction of surface-bound VSH is never completed, so that direct electron transfer from Q-CdS to EO-Y in solution does not easily occur at VSH-modified Q-CdS.

3-4 Conclusion

As a means of attaching new functionalities to Q-particles, surface modification methods are useful. As shown in this section, chemical modification of Q-CdS particles with viologen-functionalized thiol can attach the electroactivities to the Q-particles. It is also shown in this section that the amount of surface-modified VSH and RSH can be easily varied by adjusting the composition of these in the preparation bath. The results suggest that attachment of multiple functionalities to Q-CdS might be achieved by surface modification with thiol compounds having a variety of functions such as electron mediation, pH sensitivity and adsorbability. Furthermore the surface modification with

electroactive molecules that serve as electron acceptors will allow precise investigations on photoinduced charge transfers at Q-particle surfaces, as already demonstrated for chemically modified electrodes having electroactivities, because the bound acceptor are fixed at constant distance and any diffusion and adsorption problem of acceptor can be eliminated.

Conclusion

Thesis have dealt with the analysis the surface structures of size-quantized semiconductor microcrystals modified with thiol compounds, the investigations on the influence of the modified layers on the photoinduced charge transfer, and the attachment of novel functions to semiconductor microcrystals. The main results and conclusions obtained in this study are summarized as follows.

In chapter 1, the degree of surface coverage of Q-PbS with 4 hydroxythiophenol was changed by the ratio of $[Pb^{2+}]/[S^{2-}]$ used in preparation. The surface structures of Q-PbS formed by the bound modifier was successfully evaluated by comparing the chemical analyses data of the Q-PbS particles with the theoretically evaluated compositions for Q-PbS particles having modeled structures. The proposed surface structures of Q-PbS particles were rationalized by experimentally found difference both in agglomeration tendencies of particles and in the effect of the addition of Pb^{2+} ions on the rate of photoinduced reduction of methylviologen on the particles.

In chapter 2, the surface amino groups of Q-PbS which were introduced by the surface modification with 4-aminothiophenol generated positive surface charges in aqueous solution of pHs lower than 8 due to their protonation, the amount depending on the degree of surface modification of Q-PbS with 4-aminothiophenol. The electrostatic interaction between the charged surfaces of Q-PbS particles and the hole scavengers influenced the photoinduced charge transfer to methylviologen. Furthermore in the case of tartrate used as the hole scavenger, the inert electrolyte anions hindered the photoreduction of methylviologen due to the competitive adsorption of tartrate and inert anions on the surface of Q-PbS particles.

In chapter 3, Q-CdS modified with various amounts of electroactive viologen-functionalized thiol (VSH) and electroinactive alkane thiol were prepared. The surface-modified VSH was photoreduced by irradiation of Q-CdS to give both dimeric and

monomeric radical cations of the viologen, and the formation of the former was enhanced by increasing the amount of the surface-bound VSH. Kinetic analyses revealed that the rate constants for the reduction of the surface -modified VSH and for the reoxidation of the produced radical cations were independent of the amount of the VSH. Q-CdS having the higher amount of VSH showed the higher activity for electron transfer to methylene blue in solution, evidencing that the surface-bound viologen mediated electron transfers from Q-CdS to the electron acceptor in solution.

Acknowledgment

The work of this thesis was carried out under the guidance of Professor Dr. Hiroshi Yoneyama at Department of Applied Chemistry, Faculty of Engineering , Osaka University.

The author would like to express his grateful acknowledgment to Professor Dr. Hiroshi Yoneyama for his continuous guidance and encouragement throughout this work.

The author is also indebted to Professor Dr. Shunichi Fukuzumi and Professor Dr. Gen-etsu Matsubayashi for their valuable comments and suggestions.

The author desires to express his sincere thanks to Assistant Professor Dr. Hiroyuki Uchida, Yamanashi University, and Lecturer Hiroshi Inoue, University of Osaka Prefecture, for many useful suggestions for performing experiments when they were in Osaka University.

The author is much obliged to Associate Professor Susumu Kuwabata for his very useful discussion and helpful suggestions during the course of the work.

Thanks are given to the author's co-workers, Mr. Kotaro Maeda and Mr. Masahide Miyake and all other members of Yoneyama Laboratory for their kind helps and useful discussion.

Finally, the author is particularly grateful to his parents, Noboru Torimoto and Toshiyo Torimoto for their encouragement and supports.

References

1. Henglein, A. *Top. Curr. Chem.* **1988**, *143*, 113-180.
2. Henglein, A. *Chem. Rev.* **1989**, *89*, 1861-1873.
3. Steigerwald, M. L.; Brus, L. E. *Annu. Rev. Mater. Sci.* **1989**, *19*, 471-495.
4. Steigerwald, M. L.; Brus, L. E. *Acc. Chem. Res.* **1990**, *23*, 183-188.
5. Wang, Y.; Herron, N. *J. Phys. Chem.* **1991**, *95*, 525-532.
6. Kamat, P. V . *Chem. Rev.* **1993**, *93*, 267-300.
7. Weller, H. *Angew. Chem. Int. Ed. Engl.* **1993**, *32*, 41-53.
8. Yoneyama, H. *Crit. Rev. Solid State and Mater.* **1993**, *18*, 69-111.
9. Grätzel, M. *Heterogeneous Photochemical Electron Transfer* ; CRC press, Inc. ; Boca Raton, Florida, 1989.
10. Wang, Y.; Herron, N. *J. Phys. Chem.* **1988**, *92*, 4988-4994.
11. Herron, N.; Wang, Y.; Eddy, M. M; Stucky, G. D.; Cox, D. E.; Moeller, K.; Bein, T. *J. Am. Chem. Soc.* **1989**, *111*, 530-540.
12. Stramel, R. D.; Nakamura, T.; Thomas, J. K. *J. Chem. Soc., Faraday Trans. 1* **1988**, *84*, 1287-1300.
13. Rajh, T.; Vucemilovic, M. I.; Dimitrievic, N. M.; Micic, O. I.; Nozik, A. *Chem. Phys. Lett.* **1988**, *143*, 305.
14. Kakuta, N.; White, J. M.; Campion, A.; Bard, A. J.; Fox, M. A.; Webber, S. E. *J. Phys. Chem.* **1985**, *89*, 48-52.
15. Wang, Y.; Suna, A.; Mahler, W.; Kasowski, R. *J. Chem. Phys.* **1987**, *87*, 7315-7322.
16. Watzke, H. J.; Fendler, J. H. *J. Phys. Chem.* **1987**, *91*, 854-861.
17. Chang, A. -C.; Pfeiffer, W. F.; Guillaume, B.; Baral, S.; Fendler, J. H. *J. Phys. Chem.* **1990**, *94*, 4284-4289.
18. Nosaka, Y.; Yamaguchi, K.; Miyama, H.; Hayashi, H. *Chem. Lett.* **1988**, 605-608.
19. Fischer, C. -H.; Henglein, A. *J. Phys. Chem.* **1989**, *93*, 5578-5581.
20. Herron, N.; Wang, Y., Eckert, H. *J. Am. Chem. Soc.* **1990**, *112*, 1322-1326.
21. Nenadovic, M. T; Comor, M. I.; Vasic, V.; Micic, O.I. *J. Phys. Chem.* **1990**, *94*, 6390-6396.
22. Ogata, T.; Hosokawa, H.; Oshiro, T.; Wada, Y.; Sakata, T.; Mori, H.; Yanagida, S. *Chem. Lett.* **1992**, 1665-1665.

23. Chemseddine, A.; Weller, H. *Ber. Bunsenges. Phys. Chem.* **1993**, *97*, 636-637.

24. Steigerwald, M. L.; Alivisatos, A. P.; Gibson, J. M.; Harris, T. D.; Kortan, R.; Muller, A. J.; Thayer, A. M.; Duncan, T. M.; Douglass, D. C.; Brus, L. E. *J. Am. Chem. Soc.* **1988**, *110*, 3046-3050.

25. Kortan, A. R.; Hull, R.; Opila, R. L.; Bawendi, M. G.; Steigerwald, M. L.; Carroll, P. J.; Brus, L. E. *J. Am. Chem. Soc.* **1990**, *112*, 1327-1332.

26. Hayes, D.; Micic, O. I.; Nenadovic, M. T.; Swayambunathan, V.; Meisel, D. *J. Phys. Chem.* **1989**, *93*, 4603-4608.

27. Swayambunathan, V.; Hayes, D.; Schmidt, K. H.; Liao, Y. X.; Meisel, D. *J. Am. Chem. Soc.* **1990**, *112*, 3831-3837.

28. Rajh, T.; Micic, O. I.; Nozik, A. J. *J. Phys. Chem.* **1993**, *97*, 11999-12003.

29. Dameron, C. T.; Reese, R. N.; Mehra, R. K.; Kortan, A. R.; Carroll, P. J.; Steigerwald, M. L.; Brus, L. E.; Winge, D. R. *Nature* **1989**, *338*, 596-597.

30. Fischer, C. H.; Weller, H.; Katsikas, L.; Henglein, A. *Langmuir* **1989**, *5*, 429-432.

31. Eychmüller, A.; Katsikas, L.; Weller, H. *Langmuir* **1990**, *6*, 1605-1608.

32. Thayer, A. M.; Steigerwald, M. L.; Duncan, T. M.; Douglass, D. C. *Phys. Rev. Lett.* **1988**, *60*, 2673-2676.

33. Bawendi, M. G.; Kortan, A. R.; Steigerwald, M. L.; Brus, L. E. *J. Chem. Phys.* **1989**, *91*, 7282-7290.

34. Hoener, C. F.; Allan, K. A.; Bard, A. J.; Campion, A.; Fox, M. A.; Mallouk, T. E.; Webber, S. E.; White, J. M. *J. Phys. Chem.* **1992**, *96*, 3812-3817.

35. Colvin, V. L.; Goldstein, A. N.; Alivisatos, A. P. *J. Am. Chem. Soc.* **1992**, *114*, 5221-5230.

36. Marcus, M. A.; Flood, W.; Steigerwald, M.; Brus, L.; Bawendi, M. *J. Phys. Chem.* **1991**, *95*, 1572-1576.

37. Alivisatos, A. P.; Harris, A. L.; Levinos, N. J.; Steigerwald, M. L.; Brus, L. E. *J. Chem. Phys.* **1988**, *89*, 4001-4011.

38. Alivisatos, A. P.; Harris, T. D.; Brus, L. E.; Jayaraman, A. *J. Chem. Phys.* **1988**, *89*, 5979-5982.

39. Alivisatos, A. P.; Harris, T. D.; Carroll, P. J.; Steigerwald, M. L.; Brus, L. E. *J. Chem. Phys.* **1989**, *90*, 3463-3468.

40. Cheng, L. -T.; Herron, N.; Wang, Y. *J. Appl. Phys.* **1989**, *66*, 3417-3419.

41. Shiang, J. J.; Goldstein, A. N.; Alivisatos, A. P. *J. Chem. Phys.* **1990**, *92*, 3232-3233.

42. Colvin, V. L.; Alivisatos, A. P.; Tobin, J. G. *Phys. Rev. Lett.* **1991**, *66*, 2786-2789.

43. Bawendi, M. G.; Carroll, P. J.; Wilson, W. L.; Brus, L. E. *J. Chem. Phys.* **1992**, *96*, 946-954.
44. Dance, I. G. *J. Am. Chem. Soc.* **1980**, *102*, 3445-3451.
45. Hagen, K. S.; Stephan, D. W.; Holm, R. H. *Inorg. Chem.* **1982**, *21*, 3928-3936.
46. Choy, A.; Craig, D.; Dance, I.; Scudder, M. *J. Chem. Soc., Chem. Commun.* **1982**, 1246-1247.
47. Hagen, K. S.; Holm, R. H. *Inorg. Chem.* **1983**, *22*, 3171-3174.
48. Dance, I. G.; Choy, A.; Scudder, M. L. *J. Am. Chem. Soc.* **1984**, *106*, 6285-6295.
49. Dance, I. G. *Aust. J. Chem.* **1985**, *38*, 1745-1755.
50. Dean, P. A. W.; Vittal, J. J. *Inorg. Chem.* **1986**, *25*, 514-519.
51. Türk, T.; Resch, U.; Fox. M. A.; Vogler, A. *J. Phys. Chem.* **1992**, *96*, 3818-3822.
52. Türk, T.; Resch, U.; Fox, M. A.; Vogler, A. *Inorg. Chem.* **1992**, *31*, 1854-1857.
53. Nozik, A. J.; Williams, F.; Nenadovic, M. T.; Rajh, T.; Micic, O. I. *J. Phys. Chem.* **1985**, *89*, 397-399.
54. Rossetti, R.; Hull, R.; Gibson, J. M.; Brus, L. E. *J. Chem. Phys.* **1985**, *83*, 1406-1410.
55. Wang, Y.; Herron, N. *J. Phys. Chem.* **1987**, *91*, 257-260.
56. Gallardo, S.; Gutiérrez, M.; Henglein, A.; Janata, E. *Ber. Bunsenges. Phys. Chem.* **1989**, *93*, 1080-1090.
57. Miyoshi, H.; Yamachika, M.; Yoneyama, H.; Mori, H. *J. Chem. Soc., Faraday Trans.* **1990**, *86*, 815-818.
58. De Brabander, H. F.; Tombeux, J. J.; Van Pouke, L. C. *J. Coord. Chem.* **1974**, *4*, 87-92.
59. Arsenault, J. J. I.; Dean, P. A. W. *Can. J. Chem.* **1983**, *61*, 1516-1523.
60. Christou, G.; Folting, K.; Hoffman, J. C. *Polyhedron* **1984**, *3*, 1247-1253.
61. Farrington, J.A.; Ledwith, A.; Stam, M. F. *J. Chem. Soc., Chem. Comun.* **1969**, 259-260.
62. Fojtik, A.; Weller, H.; Koch, U.; Henglein, A. *Ber. Bunsenges Phys. Chem.* **1984**, *88*, 969-977.
63. Rossetti, R.; Ellison, J. L.; Gibson, J. M.; Brus, L. E. *J. Chem. Phys.* **1984**, *80*, 4464-4469.
64. Rossetti, R.; Hull, R.; Gibson, J. M.; Brus, L. E. *J. Chem. Phys.* **1985**, *82*, 552-559.
65. JCPDS International Centre for Diffraction Data 1982 No.5-592
66. Hellwege, K.-H.; Madelung, O. ed. *Landolt-Börnstein, New Series* ; Vol.III/17f pp155-162 Springer-Verlag: Berlin/Heidelberg/New York/Tokyo 1983.
67. Weller, H.; Schmidt, H. M.; Koch, U.; Fojtik, A.; Baral, S.; Henglein, A.; Kunath, W.; Weiss, K.; Dieman, E. Chem. *Phys. Lett.* **1986**, **124**, 557-560.

68. Hellwege, K. -H. ed. *Landolt-Börnstein, New Series* ; Vol.II/7 pp332 Springer-Verlag: Berlin/Heidelberg/New York 1976.
69. Bondi, A. *J. Phys. Chem.* **1964**, *68*, 441-451.
70. Hellwege, K. -H. ed. *Landolt-Börnstein, New Series* ; Vol.III/5a pp270 Springer-Verlag: Berlin/Heidelberg/New York 1971. .
71. Bird, C. L.; Kuhn, A. T. *Chem. Soc. Rev.* **1981**, *10*, 49-82.
72. Watanabe, T.; Honda, K. *J. Phys. Chem.* **1982**, *86*, 2617-2619.
73. Duonghong, D.; Ramsden, J.; Grätzel, M. *J. Am. Chem. Soc.* **1982**, *104*, 2977-2985.
74. Grätzel, M.; Frank. A. J. *J. Phys. Chem.* **1982**, *86*, 2964-2967.
75. Henglein, A.; Fojtik, A.; Weller, H. *Ber. Bunsenges. Phys. Chem.* **1987**, *91*, 441-446.
76. Spanhel, L.; Weller, H.; Henglein, A. *J. Am. Chem. Soc.* **1987**, *109*, 6632-6635.
77. Nosaka, Y.; Fox, M. A. *J. Phys. Chem.* **1986**, *90*, 6521-6522.
78. Nosaka, Y.; Fox, M. A. *Langmuir* **1987**, *3*, 1147-1150.
79. Nosaka, Y.; Fox, M. A. *J. Phys. Chem.* **1988**, *92*, 1893-1897.
80. Nosaka, Y.; Ohta, N.; Miyama, H. *J. Phys. Chem.* **1990**, *94*, 3752-3755.
81. Chang, A. -C.; Fendler, J. H. *J. Phys. Chem.* **1989**, *93*, 2538-2542.
82. Kamat, P. V. *Langmuir* **1985**, *1*, 608-611.
83. Kamat, P. V.; Patrick, B. *J. Phys. Chem.* **1992**, *96*, 6829-6834.
84. Rajh, T.; Rabani, J. *Langmuir* **1991**, *7*, 2054-2059.
85. Chandler, R. R.; Coffer, J. L. *J. Phys. Chem.* **1993**, *97*, 9767-9770.
86. Brown, G. T.; Darwent, J. R.; Fletcher, P. D. I. *J. Am. Chem. Soc.* **1985**, *107*, 6446-6451.
87. Darwent, J. R.; Lepre, A. *J. Chem. Soc., Faraday Trans. 2* **1986**, *82*, 2323-2335.
88. Frank, A. J.; Willner, I.; Goren, Z.; Degani, Y. *J. Am. Chem. Soc.* **1987**, *109*, 3568-3573.
89. Kamat, P. V.; Dimitrijevi, N. M.; Fessenden, R. W. *J. Phys. Chem.* **1988**, *92*, 2324-2329.
90. Kölle, U,; Moser, J.; Grätzel, M. *Inorg. Chem.* **1985**, *24*, 2253-2258.
91. Mulvaney, P.; Swayambunathan, V.; Grieser, F.; Meisel, D. *J. Phys. Chem.* **1988**, *92*, 6732-6740.
92. Kamat, P. V.; de Lind van Wijngaarden, M.; Hotchandani, S. *Israel. J. Chem.* **1993**, *33*, 47-51.
93. Nosaka, Y.; Ohta, N.; Fukuyama, T.; Fujii, N. *J. Colloid Interface Sci.* **1993**, *155*, 23-29.
94. Miller, C.; Cuendet, P.; Grätzel, M. *J. Phys. Chem.* **1991**, *95*, 877-886.
95. Miller, C.; Grätzel, M. *J. Phys. Chem.* **1991**, *95*, 5225-5233.
96. Becka, A. M.; Miller, C. J. *J. Phys. Chem.* **1992**, *96*, 2657-2668.

97. Becka, A. M.; Miller, C. J. *J. Phys. Chem.* **1993**, *97*, 6233-6239.
98. De Long, H. C.; Buttry, D. A. *Langmuir* **1990**, *6*, 1319-1322.
99. De Long, H. C.; Buttry, D. A. *Langmuir* **1992**, *8*, 2491-2496.
100. Chailapakul, O.; Crooks, R. M. *Langmuir* **1993**, *9*, 884-888.
101. Katz, E.; Itzhak, N.; Willner, I. *Langmuir* **1993**, *9*, 1392-1396.
102. Redepenning, J.; Tunison, H. M.; Finklea, H. O. *Langmuir* **1993**, *9*, 1404-1407.
103. Sun, L.; Johnson, B.; Wade, T.; Crooks, R. M. *J. Phys. Chem.* **1990**, *94*, 8869-8871.
104. Bryant, M. A.; Crooks, R. M. *Langmuir* **1993**, *9*, 385-387.
105. Park, G. A.; de Bruyn, P. L. *J. Phys. Chem.* **1962**, *66*, 967-973.
106. Ohtani, B.; Okugawa, Y.; Nishimoto, S.; Kagiya, T. *J. Phys. Chem.* **1987**, *91*, 3550-3555.
107. Miyoshi, H.; Mori, H.; Yoneyama, H. *Langmuir* **1991**, *7*, 503-507.
108. Kosower, E. M.; Cotter, J. L. *J. Am. Chem. Soc.* **1964**, *86*, 5524-5527.
109. Imabayashi, S.; Kitamura, N.; Tazuke, S.; Tokuda, K. *J. Electroanal. Chem.* **1988**, *243*, 143-160.
110. White, J. R.; Bard, A. J. *J. Phys. Chem.* **1985**, *89*, 1947-1954.
111. Mills, A.; Williams, G. *J. Chem. Soc., Faraday Trans. 1* **1987**, *83*, 2647-2661.
112. Mills, A.; Green, A. *J. Photochem. Photobiol. A: Chem.* **1991**, *59*, 199-208.
113. Fasman, G. D. ed. *Handbook of Biochemistry and Molecular Biology*, 3rd. edition. Physical and Chemical Data. Vol. I; CRC press: 1976. p305-351.
114. Marcus, Y. *Ion Solvation*; Wiley : New York, 1985; p108-109.
115. Willner, I.; Eichen, Y. *J. Am. Chem. Soc.* **1987**, *109*, 6862-6863.
116. Nakahira, T.; Grätzel, M. *J. Phys. Chem.* **1984**, *88*, 4006-4010.
117. Willner, I.; Eichen, Y.; Frank, A. J.; Fox, M. A. *J. Phys. Chem.*, **1993**, *97*, 7264-7271.
118. Nosaka, Y.; Yamaguchi, K.; Kuwabara, A.; Miyama, H.; Baba, R.; Fujishima, A. *J. Photochem. Photobiol. A : Chem.* **1992**, *64*, 375-382.
119. Bergmann, K.; O'Konski, C. T. *J. Phys. Chem.* **1963**, *67*, 2169-2177.
120. Moser, J.; Grätzel, M. *J. Am. Chem. Soc.* **1984**, *106*, 6557-6564.
121. JCPDS International Centre for Diffraction Data, 1982, No. 10-454.
122. Widrig, C. A.; Majda, M. *Langmuir* **1989**, *5*, 689-695.
123. Rothenberger, G.; Moser, J.; Grätzel, M.; Serpone, N.; Sharma, D. K. *J. Am. Chem. Soc.* **1985**, *107*, 8054-8059.